J. Fluid Mech. (1971), *vol.* 50, *part* 2, *pp.* 285–319
Printed in Great Britain

Experiments on internal intermittency and fine-structure distribution functions in fully turbulent fluid

By ALBERT YI-SHUONG KUO†
AND STANLEY CORRSIN
Department of Mechanics, The Johns Hopkins University

(Received 20 August 1970 and in revised form 22 March 1971)

Spatial 'intermittency' in the velocity field fine-structure of fully turbulent flow regions, first observed by Batchelor & Townsend (1949), is studied further here in grid-generated nearly isotropic turbulence and on the axis of a round jet. At large enough Reynolds numbers, appropriately filtered hot-wire anemometer signals appear intermittent as the turbulent patterns are convected past the hot wire by the mean flow. Measurements show that there is a decrease in the relative fluid volume (equal to the 'intermittency factor') occupied by fine-structure of given size as the turbulence Reynolds number is increased. They show also that, for a fixed Reynolds number, the relative volume is smaller for smaller fine-structure. The average linear dimension of the fine-structure regions turns out to be much larger than the sizes of fine-structure therein. At $R_\lambda = 110$, for example, the ratio ranges from 15 to 30, decreasing with decreasing 'eddy' size. It appears to be approaching an asymptote with increasing R_λ.

The flatness factors and probability distributions of the first derivative, the second derivative, band-passed and high-passed velocity fluctuation signals were also measured. The turbulence Reynolds numbers R_λ ranged from 12 to 830. The flatness factors of the first and the second derivatives increase monotonically with R_λ. Those of the second derivative vary with $R_\lambda^{0.25}$ for $R_\lambda < 100$, and with $R_\lambda^{0.75}$ for $R_\lambda > 300$. No indication of asymptotic constant values was observed for R_λ up to the order of one thousand.

The probability distributions of velocity fluctuations and large-scale signals are nearly normal, while the small-scale signals are not. The flatness factor of the filtered band-pass velocity signal increases with increasing frequency.

At the larger Reynolds numbers, the square of the signal associated with large wave-numbers may be approximated by a log-normal probability distribution for amplitudes when probabilities fall between 0·3 and 0·95, in limited agreement with the theory of Kolmogorov (1962), Oboukhov (1962), Gurvich & Yaglom (1967).

1. Introduction

It has been suggested for some twenty years that the 'fine-structure' of the random velocity field in a fully developed, high Reynolds number turbulent flow tends to be spatially localized. Since the viscous dissipation of turbulent kinetic

† Present address: Virginia Institute of Marine Science, Gloucester Pt., Va. 23062.

energy occurs primarily in the fine-structure ('small eddies'), this implies that the dissipation may be scattered through the fluid in a rather 'spotty' way. This spottiness of the fine-structure was first inferred by Batchelor & Townsend (1949) from the intermittent occurrence of high frequency contributions in hot-wire anemometer signals (see § 4). They used essentially high-pass filters (the effect of successive differentiations) to extract the fine-scale signals from hot-wires placed in grid-generated turbulent flows and in turbulent wakes behind cylinders. A quantitative measure of the intermittency was chosen as the amount by which the 'flatness factor' of an intermittent random variable $e(t)$, viz.

$$F \equiv \frac{\overline{e^4(t)}}{\{\overline{e^2(t)}\}^2}, \tag{1.1}$$

exceeds the values 3·0, which is appropriate to a variable with normal ('Gaussian') probability density. They found that the flatness factors of velocity derivatives were greater than 3·0, and increased with both the order of derivative and the Reynolds number of the turbulence. They therefore suggested that the energy associated with the fine-scale components is distributed very unevenly in space, and roughly confined to regions which become smaller as the eddy sizes decrease. Specifically, they said the following: "Thus the process of subdivision of the fluid into regions of strong and of weak activation will occur in a stepwise manner as the wave-number – or the order of the derivative of the velocity – increases. The various regions in which wave-numbers of order k_n are activated will all lie within regions in which wave-numbers k_{n-1} of an order of magnitude smaller than k_n are activated, and these in turn are enclosed by regions in which even smaller wave-numbers are activated." They also suggested that the linear dimensions of these active regions are large compared with the eddy sizes with which they are active, and that their mean separation is comparable with the integral scale of the turbulence.

Using a band-pass filter, Sandborn (1959) found that the fine-scale components of the turbulence in the full turbulent part of a boundary layer also tend to be spotty. Kennedy & Corrsin (1961) observed intermittency in the band-pass signals of a fully turbulent free shear layer. They also showed that such intermittency does not occur in all non-linear random processes. The flatness factors measured by Sandborn and by Kennedy & Corrsin agreed roughly with those of Batchelor & Townsend. Pond & Stewart (1965) measured the flatness factor of the first derivative of the velocity fluctuations in the wind blowing over water (in turbulence whose Reynolds number was presumably larger than those in the earlier studies), and obtained values as high as 20. Sheih (1969) also observed that the first derivative of the velocity fluctuations is intermittent in atmospheric turbulence. Gibson, Stegen & Williams (1970; see also Gibson, Stegen & McConnell 1970) observed intermittency in the first derivatives of both velocity and temperature fluctuations in the wind over the ocean. The flatness factors of the derivatives measured by these experimenters were also much larger than 3·0. Wyngaard & Tennekes (1970) have reported velocity derivative flatness factors as large as 40 in an atmospheric boundary layer.

It was remarked by Kennedy & Corrsin that, although an intermittent variable

is likely to have a high flatness factor, a high flatness factor does not necessarily imply intermittency. Therefore, the flatness factor can at most indicate the degree of intermittency of a variable already known to be intermittent by other observations. A more direct measure is the 'intermittency factor' γ, defined as the fraction of time the detection probe sees the variable in a large amplitude state.† The intermittency factor of a variable can be inferred from the flatness factor only if its probability distributions during both states are known.

An important theory of intermediate and fine-structure turbulence is given by Kolmogorov's (1941) local isotropy and similarity hypotheses (see also Batchelor 1953). This theory postulates that, irrespective of the nature of the large-scale motions of a fully turbulent region, the small-scale components of the motion are isotropic, and have statistical properties which are uniquely determined by the two parameters, the kinematic viscosity ν, and the average energy dissipation rate $\langle\epsilon\rangle$. Soon after the proposal of this similarity hypothesis, Landau & Lifshitz (1959) raised doubt about its validity because of the possible presence and importance of large fluctuations in the instantaneous energy dissipation rate.

This concern attracted little attention for several years. Eventually, Oboukhov (1962), Kolmogorov (1962), Corrsin (1962), Novikov (1963), Novikov & Stewart (1964), Yaglom (1966), Gurvich & Yaglom (1967), Tennekes (1968) and Saffman (1970) made some attempts to include this phenomenon in theoretical analyses.

In their attempt to modify the original Kolmogorov's similarity hypothesis, Oboukhov (1962) and Kolmorogov (1962) introduced the concept of a 'pure ensemble'. They further assumed that the logarithm of $\tilde{\epsilon}_r$, the average energy dissipation rate over a volume of linear dimension r, had a normal distribution, and they thereby arrived at modified expressions for the velocity 'structure function' and skewness factors.

Using the idea of successive subdivision of volume, Gurvich & Yaglom (1967) attempted to devise a more basic derivation of the log-normal law by means of a mathematical description for the consequence of the cascade process of sequential breakdown of turbulent eddies. They reached the conclusion that any non-negative quantity governed by fine-scale components has a log-normal distribution with variance σ^2 given by

$$\sigma^2 = A + \mu \ln(\mathscr{L}/\eta), \tag{1.2}$$

where A is a constant depending on the macrostructure of the flow, and μ is a universal constant. Saffman (1970) has arrived at a similar result by a somewhat different route.

Corrsin (1962) suggested a very explicit model, with energy dissipation localized in randomly distributed thin sheets (or slabs). He assumed slab thickness on the order of Kolmogorov microscale and spacing on the order of the integral scale. His model predicts that the flatness factor of the first derivative of velocity fluctuations increases with $R_\lambda^{\frac{3}{2}}$. Tennekes (1968) modified this idea by suggesting a model of randomly distributed 'vortex tubes', with diameter on the order of Kolmogorov microscale and spacing on the order of Taylor microscale λ. This predicts that the flatness factor increases linearly with R_λ.

† First defined by Townsend (1948) in his study of the boundary between a turbulent wake and a (potential flow) 'free stream'.

The experiments reported here were first an attempt to find out unequivocally whether spatial localization of fine-structure occurs (still a controversial question in 1968 when these experiments were begun). With the phenomenon confirmed, we set out to extend the Batchelor–Townsend (1949) data indicating dependence on Reynolds number, and the Batchelor–Townsend and Kennedy–Corrsin (1961) evidence for dependence on wave-number. Finally, we wanted to determine the extent to which positive random variables characterizing the fine-structure showed log-normal probability distributions, as reported by Gurvich & Zubkovskii (1963), Sheih, Tennekes & Lumley (1971), Stewart, Wilson & Burling (1970) and Gibson, Stegen & Williams (1970).

2. Experimental equipment and procedures

2.1. *Aerodynamic facilities*

(i) *Grid-generated turbulence* ($R_\lambda = 12{\cdot}6$, $21{\cdot}8$). The wind tunnel used to generate these two flow fields was that used by J. C. Bennett (private communication). It has a 12×18 in. test section with a closed return. The grids are both of solidity about 0·34 with mesh sizes $M = \frac{1}{6}$ and $\frac{1}{2}$ in. Measurements were made at $x/M = 42$, and mean speed $\overline{U} = 20{\cdot}6$ ft sec^{-1}. Reynolds numbers R_λ and 'Kolmogorov scale frequencies' f^* were evaluated from the turbulent energy decay rates and turbulent intensities measured by Bennett. f^* is the frequency observed by the fixed hot-wire probe when a disturbance of size equal to the Kolmogorov microscale, $\eta \equiv (\nu^3/\langle\epsilon\rangle)^{\frac{1}{4}}$, is convected past by the mean flow:

$$f^* = \overline{U}(\langle\epsilon\rangle/\nu^3)^{\frac{1}{4}}/2\pi. \tag{2.1}$$

(ii) *Grid-generated turbulence strained by slight contraction to make it more nearly isotropic* ($R_\lambda = 39$ to 150). The wind tunnel was that used by Comte-Bellot & Corrsin (1966). It has a closed circuit and a test section 32 ft long, 3×4 ft in cross-section. The grids used are of square rod, square mesh, bi-plane construction. The mesh sizes are 1, 2 and 4 in., and the solidity 0·34. Measurements were made at x/M equal to or greater than 42, and mean speeds of 26·3, 41·7 and 83·4 ft sec^{-1}. The turbulence decay and scales were reported by Comte-Bellot & Corrsin.

(iii) *Round jet* ($R_\lambda = 350$ to 830). The jets were generated by two single-stage axial fan units in tandem exhausting directly through nozzles with diameters of 6 and 2·53 in., with contraction area ratios of 6·67 : 1 and 37·5 : 1. Measurements were made on the jet axes, fifty orifice diameters from the nozzles. The mean speeds were 8·0, 10·0 and 19 ft sec^{-1} at the measurement points. The turbulent characteristics at $R_\lambda = 830$, the largest value, were measured by Gibson (1963). Cases with lower Reynolds numbers were obtained by lowering the speed and/or reducing the orifice diameter. Reynolds numbers and Kolmogorov-scale frequencies were estimated from those at $R_\lambda = 830$ by assuming similarity and local isotropy of the turbulence in the jet.

2.2. *Hot-wire anemometers*

Velocity fluctuations in the grid-generated turbulence were measured with Shapiro & Edwards constant current hot-wire anemometer units. Some calibrations are given by Comte-Bellot & Corrsin (1971). The compensation circuit

settings were determined with the square wave injection technique (Kovasznay 1947). Wire overheat ratios of 0·3 to 0·4 were used. Owing to the smallness of the turbulence levels (about 2 %), the amplifier output (a.c. coupled) is very nearly linearly proportional to the velocity fluctuations.

For the measurements in jets, a Disa type 55D01 constant temperature anemometer was used in conjunction with a Disa type 55D10 linearizer. An overheat ratio of 0·7 and a linearizer exponent setting of 2·22 were found to yield a linear calibration curve. The linearizer output was filtered by a Disa type 55D25 auxiliary unit, which is an amplifier with separately adjustable low and high cut-off frequencies. The output of the auxiliary unit is then essentially proportional to streamwise velocity fluctuations. For discussion of possible residual non-linear effects at large turbulence levels, see Rose (1962) and Heskestad (1965*a*).

Hot-wire probes were made of jeweller's broaches encased in Nu-Weld dental cement, with a main shaft of $\frac{1}{4}$ in. stainless steel tube. Only the streamwise turbulent velocity component was measured, with a single wire set normal to the mean flow. All data were taken with platinum-(10 %) rhodium wire etched from Wollaston type after the silver coating had been soldered to the tips of the jeweller's broaches. Wires 0·00005 in. in diameter and 0·01 to 0·015 in. long were used, except for measurements of band-pass signals of grid-generated turbulence. There, in order to increase the signal-to-noise ratio of band-pass signals with large mid-band frequencies, 0·000025 in. wires, 0·01 in. long, were used without thermal compensation. The reciprocal of the thermal time constant of this wire is about 6·5 kHz, which is higher than the Kolmogorov-scale frequency ($f^* = 5{\cdot}9$ kHz) of the field in which these wires were used.

2.3. *Fine-structure signal acquisition circuits*

Three kinds of circuits were used to extract fine-scale signals from the outputs of the anemometer amplifiers: differentiation circuits, band-pass filters, and high-pass filters.

An RCA CA3010A integrated circuit operational amplifier was used to obtain the first derivative. The output was differentiated again, if desired, with a Disa type 55A06 differentiator with nominal time constant of 0·2 msec. In this experiment, differentiation tends to reduce signal-to-noise ratio; a Krohn–Hite model 330-M filter with separately adjustable low and high cut-off frequencies and 24 db octave^{-1} cut-off at both ends was used to attenuate the unwanted high frequency signal and noise. A block diagram is shown in figure 1. When the first derivative was measured, the filter was connected directly to the output of the CA3010A. The frequency responses are shown in figure 2.

The Krohn–Hite filter was used to obtain band-pass signals with various mid-band frequencies f_m and with bandwidths $\Delta f/f_m$ greater than 0·5, where

$$\Delta f = f_h - f_l, \quad f_m = (f_h f_l)^{\frac{1}{2}},$$

f_h and f_l are the upper and lower 3 db points of the band-pass filter, respectively. To realize a filter with relative bandwidth less than 0·5, a Dytronics Model 720 filter was used in cascade with the Krohn–Hite filter. The Dytronics filter has

three constant-percentage bandwidth settings, all less than 0·5, the minimum bandwidth of Krohn–Hite filter (given in Comte-Bellot & Corrsin 1971). The cascade of the two filters was necessary because of the insufficient attenuation rate on the tails of the frequency response curves of the Dytronic filter. The Krohn–Hite filter characteristics are given in the instruction manual.

Four-pole Butterworth high pass filters with amplifiers were also used to extract fine-structure signals. The last stage amplifier has a 6 db octave^{-1} high-frequency cut-off to reduce the noise. The frequency response is shown in figure 3.

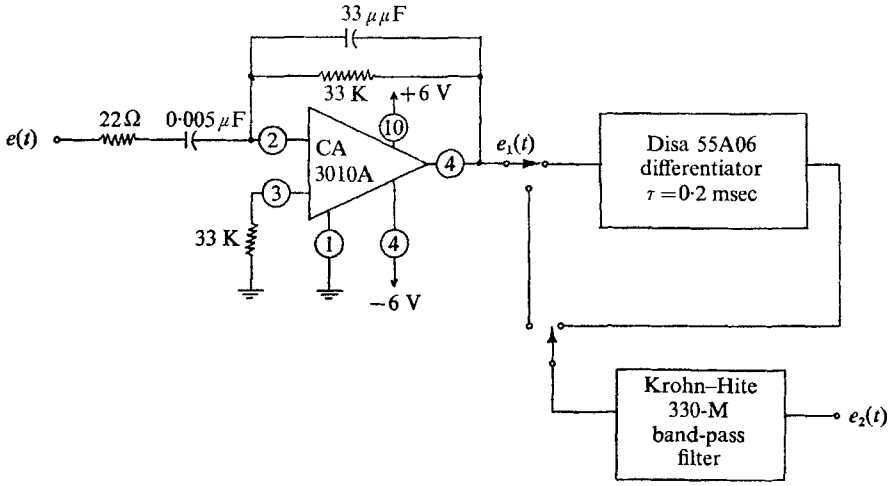

FIGURE 1. Differentiation circuit.

2.4. *Flatness factor measurements*

Figure 5 shows the system block diagram for measuring the flatness factor of a random voltage $e(t)$. A Philbrick operational amplifier (response down 1 db at 20 kHz) was used to raise the input signal to a desirable level. Its output r.c. circuit eliminated any d.c. level due to drift and improper bias.

A signal proportional to $e^2(t)$ was obtained with a Philbrick Model Q3-M1P or a GPS Model MU-405 multiplier, whose frequency responses and static transfer characteristics are shown in figures 4 and 5. The time average† was taken with a Kramer timer and SOS Model SI-100 integrator. The integrator output Q_1 was proportional to $\overline{e^2}$, and was read with a Cubic Model V-46P digital voltmeter. With switches at positions 2, the multiplier output was squared and partially averaged by vacuum thermocouples, then amplified with Honeywell Model A20B d.c. amplifier to a desirable amplitude before entering the integrator. Thus, the voltmeter would read a value proportional to $\overline{e^4}$. The flatness factor was then calculated by the formula,

$$F = K\frac{Q_2}{Q_1}, \tag{2.2}$$

† In this experiment, the random variables are stationary and time integral scales are non-infinite, which is a sufficient condition for an ergodic property (see Leipmann 1952). Therefore, the time averages of the experiment may be compared with the ensemble averages commonly used in theoretical analyses.

where the constant K was determined with the use of sine waves and Gaussian 'noise' as $e(t)$. The flatness factors of sine wave and Gaussian noise are 1·5 and 3·0, respectively, and the constants determined with them agreed within 2%.

The vacuum thermocouple circuit consists of a variable protective resistor in series with five vacuum thermocouples with heaters connected in parallel and thermocouples connected in series. The use of multiple vacuum thermocouples not only increases the output capability, but also helps to average out the randomly 'imperfect' (non-square) characteristics of individual ones. The collective transfer characteristics was satisfactory (figure 7).

The Honeywell d.c. amplifier has a frequency response flat up to 20 kHz (−1 db) and a d.c. drift negligible with respect to signal level.

The integrator has an inherent error voltage E_r across the input terminals, which depends on the output readings as shown in figure 6. During the period of integration, this error voltage causes a current flow in the input circuit, thus yielding an error at the output, or a 'drift' in cases when the output should be zero. The drift characteristics are also shown in figure 8, with various sources and source impedances. Since the error voltage changes sign at the mid-scale of the output reading, the error was minimized by setting the initial reading at such a magnitude that the initial (before integration) and the final (after integration) readings were roughly symmetric about the mid-scale.

Owing to the finite useful 'ceiling-to-floor ratio' of the multipliers' transfer characteristics, their input signal levels cannot be arbitrarily set. If the input signal is too high, portions of the signal will be clipped. If the input signal is too low, a large part of the signal will be smaller than the levels above which the multipliers square properly. Figure 9 shows the effect on the measured flatness factors of the input amplitude. The values at the level parts of the curves were considered to have least errors, and used as 'true' flatness factors. These values were also obtained by setting the amplifier gains such that the multipliers' outputs were observed to be barely clipped on an oscilloscope. This 'barely clipped' criterion was then used to set the amplifier gain.

2.5. *Probability measurements*

The probability distribution functions were measured with a QTL Model 317 amplitude distribution analyzer, which measured the relative time duration an input signal exceeds some reference level. Numerical differentiations of the curves faired to the measured points were performed with I.B.M. Model 7094 computer to obtain probability density functions. More than sixty points were taken from each faired curve as input data for the computer program. Triads of adjacent points were fitted with a second-order curve, whose secant slope was then evaluated. This slope equals that of the midpoint tangent. A test of this differentiation technique made on a normal distribution curve showed precision better than that of the data.

2.6. *Intermittency measurements*

Townsend's technique for measuring the intermittency of an intermittent signal $e(t)$ was used. It involves generating a signal $I(t)$ that is a random square wave, equal to a constant (e.g. 1·0) when $e(t)$ is at its 'higher state', and zero when $e(t)$

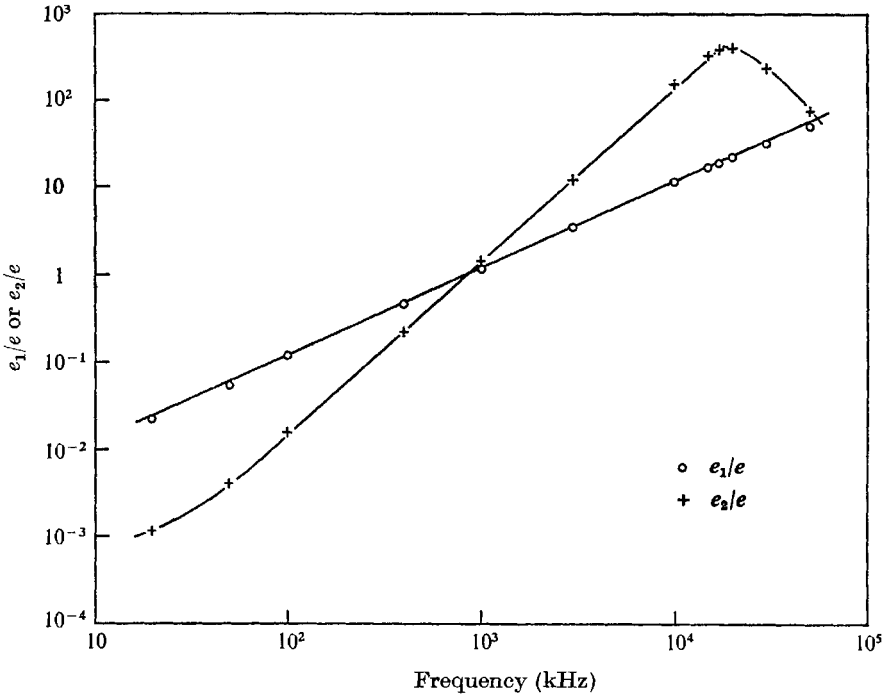

FIGURE 2. Frequency response, differentiation circuit: K–H filter (24 db octave^{-1} cut-off at both ends) set at 1 Hz–20 kHz.

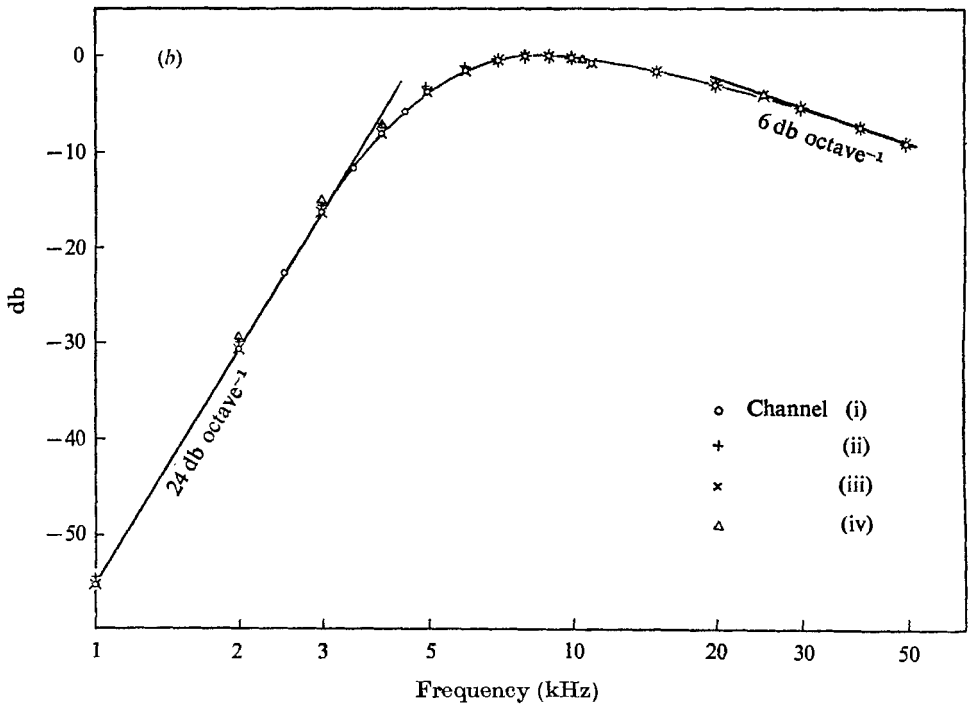

FIGURE 3. Frequency response, high-pass Butterworth filter with amplifiers.

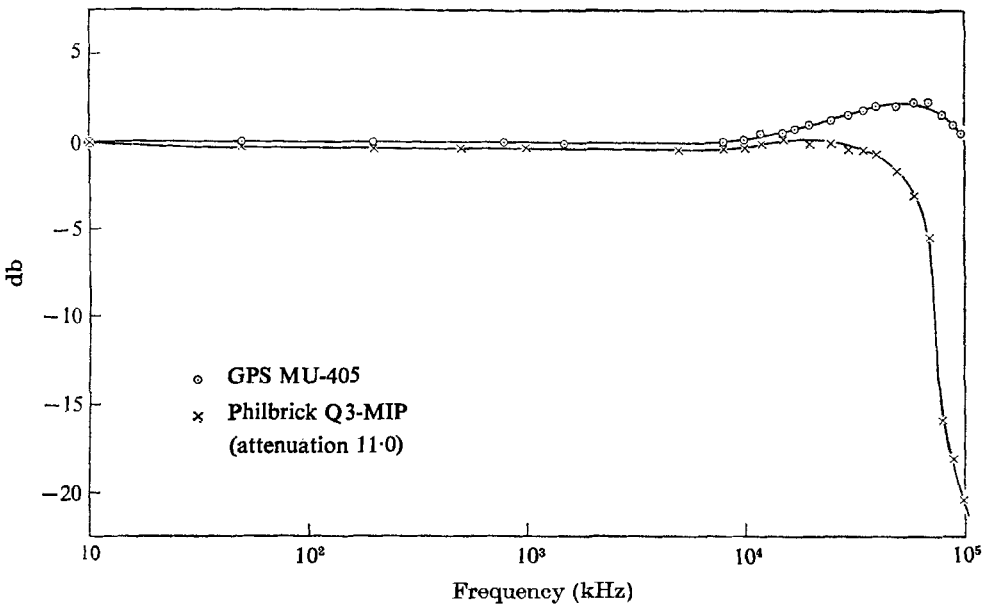

FIGURE 4. Frequency response, multipliers used as squaring circuits.

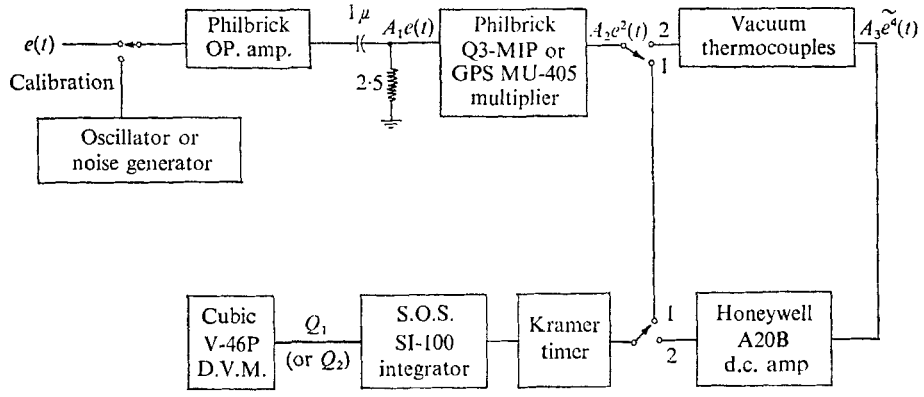

FIGURE 5. Block diagram of the flatness-factor measuring devices. ($\sim$ means short time average, which is due to time constant of vacuum thermocouples).

is at its 'lower state'. The time average of $I(t)$ is the 'intermittency factor' of $e(t)$. Electronic circuits to generate the intermittent signal $I(t)$ have been developed and used in experiments to study the turbulent-non-turbulent interfaces at a 'free' fluid boundary. A detailed historical account may be found in Kohan (1969).

In the present investigation, the intermittency circuits were built with the same operating principle as earlier ones. A block diagram, indicating the operations on a hypothetical signal, is given in figure 10(*a*), the actual circuit in figure 10(*b*). The incoming voltage $e(t)$ from the filter is rectified by the rectifier circuit,

with the variable resistor to assure equal gain at both signal polarities. To reduce noise, the rectified signal is made to work against a bias at the base of the transistor Q 1, which works as an emitter follower. The pair of transistors Q 2 and Q 3 constitutes a level comparator, with reference level controlled by the 20-turn trim pot R 2.

The signal at the collector of Q 2 is roughly a random square wave, as shown at the output of the first level comparator in figure 10 (*a*), where the finite transition

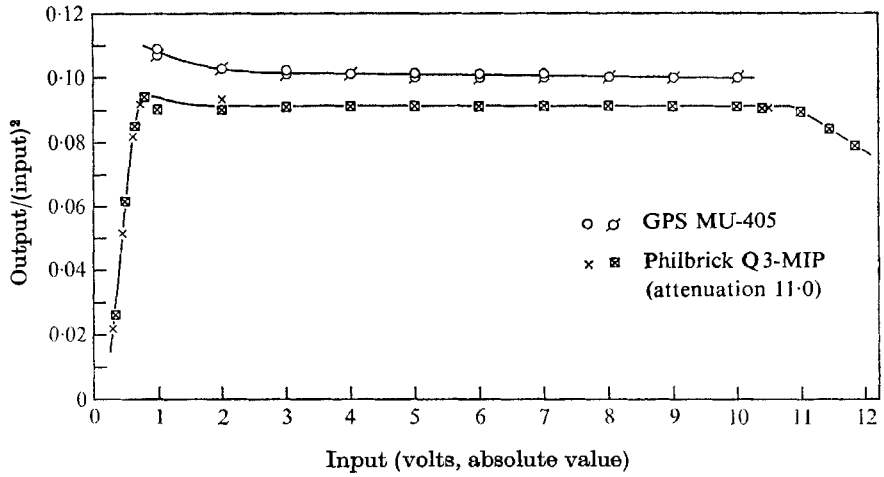

FIGURE 6. Static transfer characteristics of multipliers used as squaring circuits.

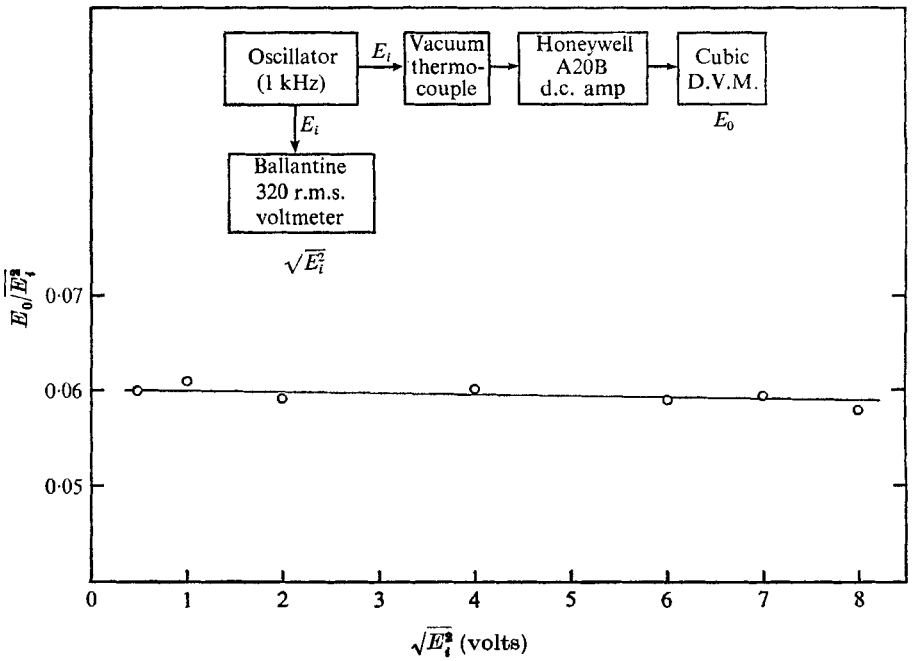

FIGURE 7. Transfer characteristics of vacuum thermocouple array.

time between two states has been exaggerated. The finite transition time is due to the need for a 0·15 volt excursion at the base voltage of transistor Q2, in order to change it from cut-off to saturation, or *vice versa*. This signal also has a problem of 'drop-out'. During the period when $e(t)$ is entirely at its 'higher state', the magnitude of the rectified signal will nevertheless fall below the comparator reference level at random times, giving a spurious zero region in $I(t)$. An r.c. circuit is used to smooth over such drop-outs. The time constant of the r.c. circuit is set approximately at $(2\pi f_p)^{-1}$, where f_p is the frequency at which the spectrum of $e(t)$ is maximum. Clearly, such smoothing causes some error at the transition points in $I(t)$.

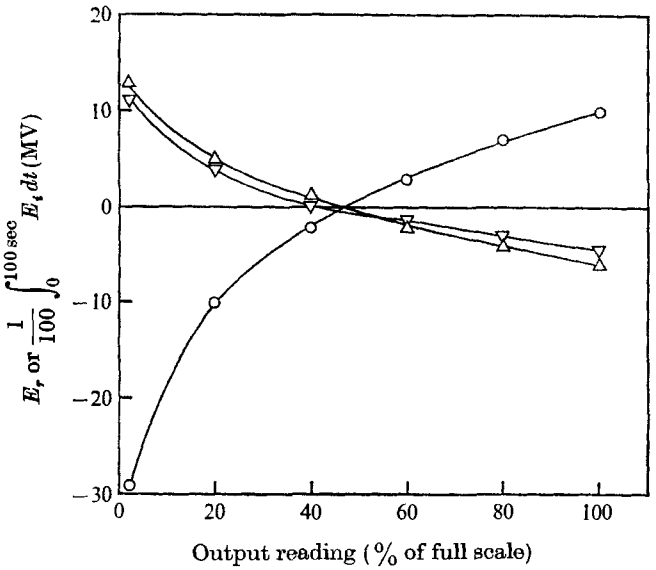

FIGURE 8. Drift characteristics of integrator: △, E_i (i) shorted, or (ii) from output of oscillator (output impedance 630 Ω), either without signal, or with 100 CPS sine wave, 1 volt peak to peak; ▽, E_i from Scott 811A noise generator (output impedance 350 Ω) either with or without signal; ○, E_r, error voltage across input terminals.

The d.c. level of the smoothed signal is then blocked by another r.c. circuit before the signal passes through emitter follower Q4 and the second level comparator. The smoothed signal is obtained from the connector S2 and displayed with $e(t)$ on a Hughes Model 104D dual trace storage oscilloscope. By comparing the traces of $e(t)$ and the signal from S2, it is possible to adjust R2 until the latter follows the former closely.

The transistors Q5 and Q6 constitute the second-level comparator that transforms the smoothed signal into a random square wave. The smoothed signal has a sufficiently high magnitude so that the level comparator output can be taken to be a square wave with rise and fall times small compared with the typical period of an on–off cycle. The transistor Q7 brings the two states of the random square wave to zero and about 3 volts. The signal from the connector S3 is then displayed with $e(t)$ on the storage oscilloscope; R4 is adjusted until the two correspond closely. Then the signal at S3 is $I(t)$.

Two statistical properties of $I(t)$ were measured: the average pulse frequency n and the intermittency factor γ. The average pulse frequency was measured by counting the pulses of $I(t)$ with a CMC Model 226B universal counter-timer. To measure intermittency factor, a 500 kHz sine wave and $I(t)$ were fed to a NAND gate made of an RCA 2205D integrated circuit. The average pulse frequency of the NAND gate output was measured with the counter, and its ratio to 500 kHz is the intermittency factor.

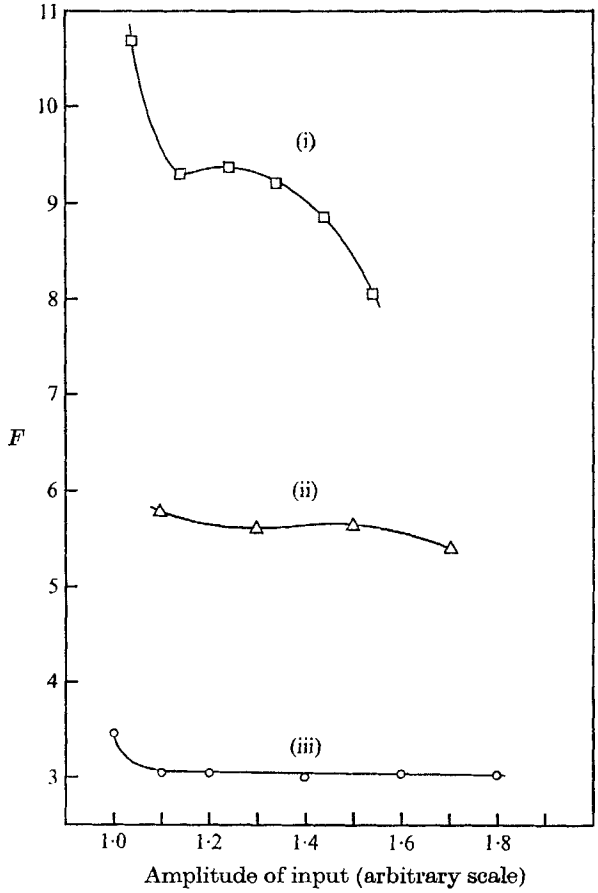

FIGURE 9. Apparent flatness factor *vs.* amplitude of input: (i) $\partial^2 u/\partial t^2$, $R_\lambda = 110$, $f_c = f^*$, $F = 9{\cdot}30$; (ii) $\partial u/\partial t$, $R_\lambda = 150$, $f_c = f^*$, $F = 5{\cdot}60$; (iii) signal from Scott noise generator (ASA), $F = 3{\cdot}0$.

The measured apparent values of γ and n depended on the settings of the reference levels of the level comparators. The decisions on optimum levels were made by careful comparison between the input and output signals displayed on the storage oscilloscope. A repeatability with $\pm 5\,\%$ was achieved. A more detailed investigation was made on the particular case of the grid-generated turbulence with $R_\lambda = 110$. The reference levels yielding $\gamma = 0{\cdot}30$ for its high-pass signal were checked to be optimum by the following experiment. After the reference levels were set according to visual comparison of the displayed signals,

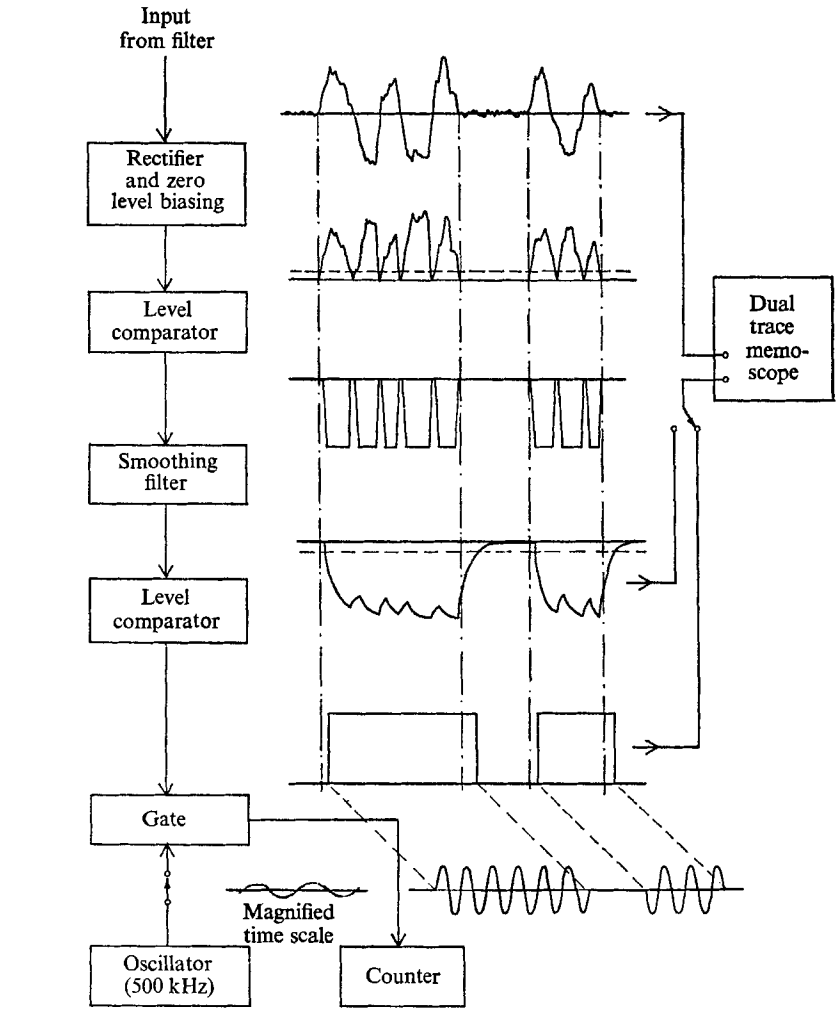

(*a*)

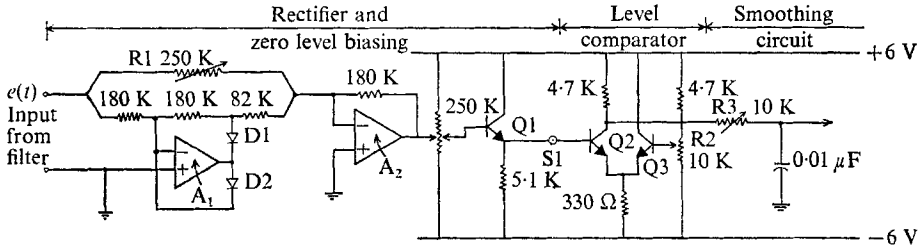

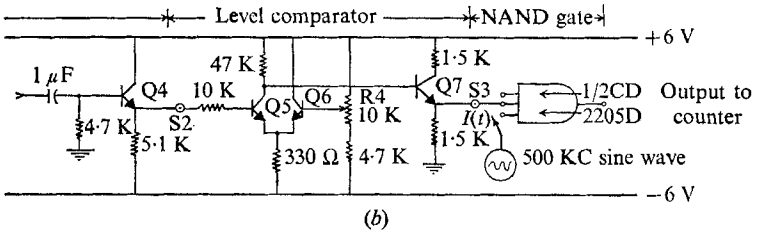

(*b*)

FIGURE 10. Intermittency-measuring device: (*a*) block diagram, and operations on a hypothetical signal; (*b*) circuit diagram.

the turbulence-generating grid was removed from the wind tunnel, while the mean flow velocity and the settings of all instruments were kept unchanged. The intermittency circuit output remained at zero, showing that the reference levels were large enough to eliminate noise effects. Then the gain of the hot-wire anemometer amplifier was increased by one step (a factor of $\sqrt{2}$), and $I(t)$ was observed to be at its 'on state' occasionally; this suggested that the reference levels could not be lowered appreciably without getting spurious pulses.

3. Experimental results

3.1. *Observation of fine-structure intermittency*

Approximate visualization of the instantaneous spatial structure of the turbulent velocity field is given by an oscillogram of the hot-wire anemometer output. The interpretation of time history at a fixed point as instantaneous spatial structure is a 'Taylor approximation', which turns out to be very good over the full spectral range for the small turbulence level case (the grid-generated turbulence with $\langle u^2\rangle^{\frac{1}{2}} \approx 0{\cdot}02\overline{U}$; see Comte-Bellot & Corrsin 1971). It is only fair in the large turbulence level, inhomogeneous structure of the jet axis where $\langle u^2\rangle^{\frac{1}{2}} \approx 0{\cdot}2\overline{U}$ (see Heskestad 1965*b*; Fisher & Davies 1964; Lumley 1965; Champagne, Harris & Corrsin 1970).

The transduction of velocity fluctuation into voltage allows easy selection of restricted domains in the wave-number space by filtering in the frequency domain. Ideally, we should like to be able to select turbulence in a limited wave-number *magnitude* range, a spherical shell in wave-number space. The one-dimensional character of our system, however, gives us a limited domain which is an infinite slab perpendicular to the mean flow direction, hence the k_1-axis. A perfect band-pass filter, rejecting all signals outside the band ω_a-to-ω_b, will therefore deliver velocity structure lying in a slab between $k_{1a} = \omega_a \overline{U}^{-1}$ and $k_{1b} = \omega_b \overline{U}^{-1}$. This contains velocity structure with all wave-number magnitudes $k \geqslant k_{1a}$. Nevertheless, the voltage thus obtained is fairly local in wave-number space.

Figure 11(*a*) (plate 1) shows typical oscillograms of band-pass and high-pass signals from a hot wire in the grid-generated turbulent flow field at moderate Reynolds number, $R_\lambda = 110$. The low frequency signal is more or less uniformly distributed in time, while the high frequency signals appear to be intermittent. With Taylor's approximation, high frequency signals correspond to the velocity fluctuations associated with the fine-scale components of motion, as it is convected past the hot wire by the mean flow. Therefore, the intermittency of the high frequency signal implies localization of the fine-structure in space.

Figure 11(*b*) (plate 1) shows the oscillograms of the total turbulent signal and of its first and second time derivatives. The derivative signals emphasize the fine-scale components, and their 'crest factors' appear to increase as the order of derivative increases. However, they do not appear explicitly intermittent as the sharply band-passed high frequency signals do. This is partly because the Reynolds number of the turbulence is not high enough to remove the spectrum of derivative signals far away from that of the energy containing eddies, which are more or less uniformly distributed in space. It is also partly because the derivative

operation does not cut out the low frequency parts of the signal as completely as does the filter system described earlier.

Since the viscous dissipation of turbulent kinetic energy occurs primarily in the fine-structure, fine-structure intermittency implies that the energy dissipation will occur in a spatially 'spotty' way if the Reynolds number of the turbulent flow is high enough.

3.2. *Flatness factor*

The flatness factor F of a random variable e is defined as

$$F \equiv \frac{\langle e^4 \rangle}{\langle e^2 \rangle^2} = \frac{\int_{-\infty}^{+\infty} a^4 P_e(a)\, da}{\left\{\int_{-\infty}^{+\infty} a^2 P_e(a)\, da\right\}^2}, \tag{3.1}$$

where $P_e(a)$ is the probability density of $e(t)$. Since the fourth moment depends more heavily on the large values of e than does the second moment, the flatness factor is a measure of the relative extent of the skirts of the probability density curve. A random variable with normal probability density has a flatness factor of 3·0. $(F-3{\cdot}0)$ is called the 'kurtosis'. The roughly normal variable, whose probability density function is more peaked in the neighbourhood of the mean than is a normal density of the same standard deviation, will have positive kurtosis. So will a two-state variable with zero 'lower state' and normal 'higher state.

As seen in (3.1),the probability density function uniquely determines the flatness factor, but the converse is of course not true. Though an intermittent variable is likely to have a large flatness factor, a large flatness factor does not necessarily imply intermittency. Therefore, flatness factor can be used to indicate the degree of intermittency only if it is known by other observations that the variable is intermittent. Batchelor & Townsend (1949) suggested a relation between flatness factor and intermittency factor:

$$\gamma = 3{\cdot}0/F, \tag{3.2}$$

which assumes the intermittent variable varies with a normal probability distribution for a fraction γ of the total time (the 'higher state'), and is zero for the remainder of the time (the 'lower state').

Having observed fine-structure intermittency on the oscillograms (as described in § 3.1), we could use measured flatness factors of the velocity derivatives and band-pass signals to indicate the degree of intermittency, as well as the degree of deviation from normal distribution. The flatness factors of the velocity fluctuations u were also measured and found to be quite close to 3·0, as has been reported by other investigators.

The noise spectrum of a compensated hot-wire signal ordinarily increases with frequency (because the basic noise spectrum is ordinarily flat), while the energy spectrum of the turbulence decreases sharply with increasing frequency in the high frequency range. Differentiation accentuates the high frequencies present in the total signal, so it tends to reduce the signal-to-noise ratio. Therefore, some kind of low-pass filter is necessary to cut off the highest frequencies, at which the noise completely masks the signal.

The effect of a sharp (24 db octave^{-1}) high cut-off frequency on the flatness factors of the first and the second derivatives of the signal are shown in figures 12(*a*), (*b*) respectively. The flatness factors tend to increase with increasing cut-off frequency, at least up to the Kolmogorov scale frequency. The rate of increase is greater for the second derivative than for the first, and for the higher Reynolds number flow; both differentiation and R_λ give relatively more high frequency

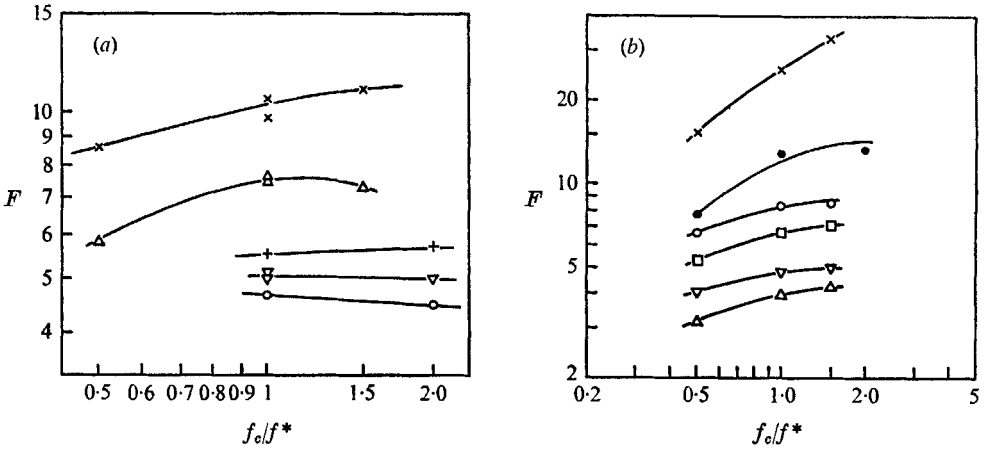

FIGURE 12. Flatness factors as functions of high cut-off frequency f_c/f^*.

	(*a*) $\partial u/\partial t$		(*b*) $\partial^2 u/\partial t^2$	
	R_λ	f^* kHz	R_λ	f^* kHz
Grid-generated turbulence	○ 49	8·7	△ 12·6	3·66
	▽ 72	6·7	▽ 39	2·40
	+ 110	5·9	□ 72	6·70
			○ 140	13·8
Jet axis	△ 350	1·78	● 350	1·78
	× 830	6·55	× 830	6·55

'energy'. This tendency agrees with the observation that the flatness factors of band-pass signals increase with frequency, to be discussed later. If the cut-off frequency is too high, however, the output includes more additional noise than signal, and the flatness factor begins to level off, since the noise is approximately normal, and will eventually decrease.This levelling-off tendency is observed particularly in the first derivative signals of lower Reynolds number flows, which have less high frequency 'energy'.

The measured flatness factors of the first and the second derivatives are shown in figures 13, 14 as functions of R_λ, which ranged from 12 in a grid-generated turbulence to 830 on the axis of a round jet. To be consistent for differing Reynolds number flows, the cut-off frequencies of the low-pass filters were set at the frequencies of the Kolmogorov microscales.† This cut-off is well above the derivative spectral peak. Some measurements by other investigators are included in figures 13, 14 for comparison and extension.

† That is, the frequency $f^* \equiv \bar{U}/2\pi\eta$ corresponding to the convection of η-scale past the hot wire. $\eta \equiv (\nu^3/\langle\epsilon\rangle)^{\frac{1}{4}}$.

Since Batchelor & Townsend (1949) did not specify the cut-off frequency of their circuits, an effort was made to discover their procedure by matching their results. By repetition of their experiments, we established the strong likelihood that they used a single cut-off frequency for all cases. The flatness factors as a function of R_λ, with various constant cut-off frequencies, were compared with the Batchelor–Townsend data. Results with cut-off frequency at 3·5 kHz were found to agree best with their data. We then adjusted their second derivative data to the values consistent with cut-off at f^*. Their first derivative data were not adjusted because the variation of the flatness factor is comparatively small at these low Reynolds numbers.

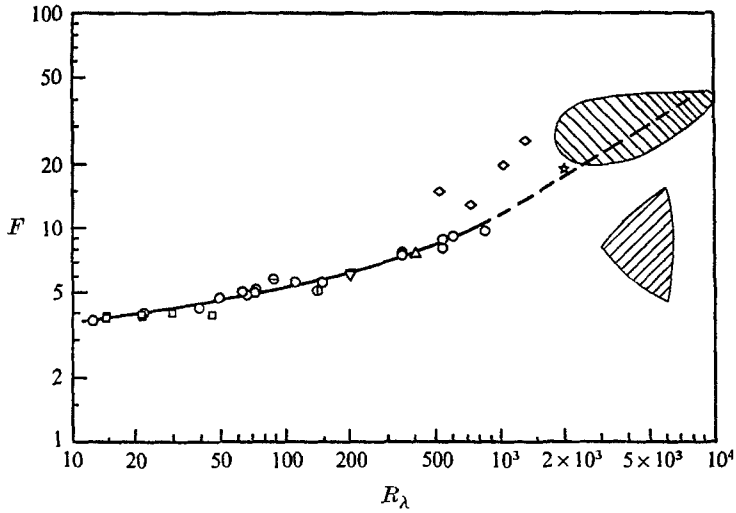

FIGURE 13. Flatness factor of $\partial u/\partial t$ as function of Reynolds number R_λ, with $f_c = f^*$. ⊖, $f_c = 1{\cdot}2f^*$; ⊕, $f_c = f^*$.

- ○ Present study.
- □ Batchelor & Townsend (1949), not corrected for cut-off.
- △ Wygnanski & Fiedler (1970).
- ▽ Wyngaard (1967), two points, $f_c = 1{\cdot}4f^*$.
- ✲ Pond & Stewart (1965), R_λ established by Shieh *et al.* (1971).
- ◇ Gibson, Stegan & Williams (1970).
- ▨ Shieh *et al.* (1971).
- ▧ Wyngaard & Tennekes (1970), Comte-Bellot (1965).

Batchelor & Townsend (1949) inferred from the original Kolmogorov similarity hypothesis that the limiting values of the flatness factors of velocity derivatives should be independent of the large-scale properties of the turbulence, and should reach universal constant values at large enough Reynolds numbers (see also Batchelor 1953). The flatness factor of the first derivative is presented in figure 13. In addition to the new data for isotropic grid-turbulence and round jet, we have included a point by Wygnanski & Fiedler (1970) in a plane shear zone, a point by Wyngaard (1967) in a curved channel, two points by Comte-Bellot (1965) in a plane channel, four points estimated from the data of Gibson, Stegen & Williams (1970) and a single point from Pond & Stewart (1965) with R_λ estimated by Sheih, Tennekes & Lumley (1971). In addition, we have added

two large shaded areas indicating clouds of points from Wyngaard & Tennekes (1970) and from Sheih, Tennekes & Lumley (1971).

The Wyngaard–Tennekes data have been weighted more heavily in drawing the curve. The Sheih–Tennekes–Lumley values are well below those found typically by several other investigators. The R_λ values assigned to the Gibson–Stegen–Williams data are quite uncertain, having been estimated by assuming that $R_\lambda \approx \lambda(1{\cdot}3u_*)/\nu$, where u_* is the 'friction velocity', $[\tau_0/\rho]^{\frac{1}{2}}$†. Here τ_0 is shear stress at the boundary and ρ is density.

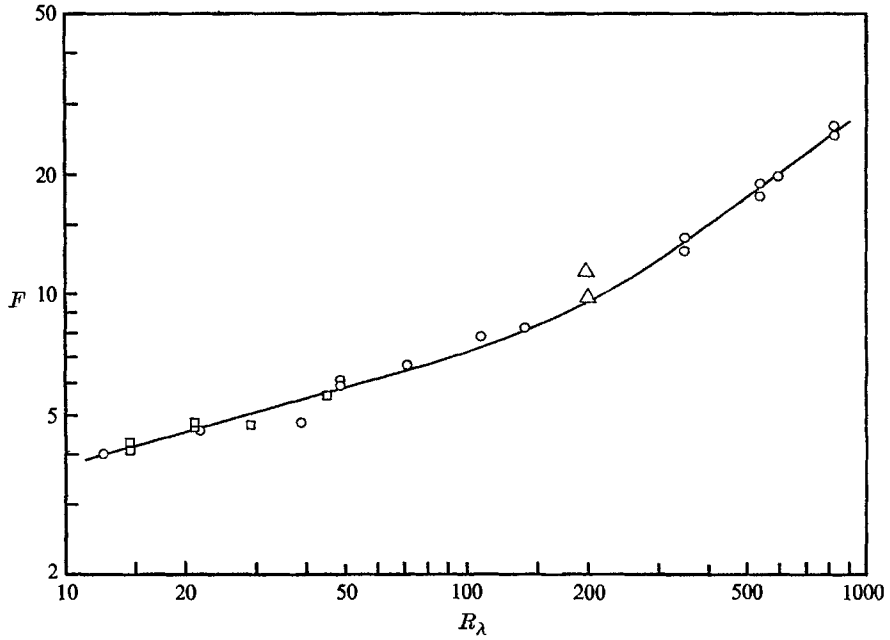

FIGURE 14. Flatness factor of $\partial^2 u/\partial t^2$ as function of Reynolds number R_λ, with $f_c = f^*$.

○ Present study.
□ Batchelor & Townsend (1949), adjusted to $f_c = f^*$.
△ Wyngaard (1967), $f_c = 1{\cdot}4f^*$.

The flatness factor of the first derivative increases like $R_\lambda^{0.2}$ at Reynolds numbers below 200. Then, following a transition zone up to 500, they may increase more rapidly (the line is drawn for $R_\lambda^{0.6}$), instead of levelling off.

In figure 14, the flatness factor of the second derivative $\sim R_\lambda^{0.25}$ up to $R_\lambda \approx 100$, and $\sim R_\lambda^{0.75}$ for $R_\lambda > 300$. Apparently, the flatness factors of the derivatives show no sign of approaching constants at Reynolds numbers R_λ of the order of thousands, which is believed to be high enough for the universal similarity hypothesis to apply (Corrsin 1958; Bradshaw 1967).

In fact, it is doubtful that the flatness factors of the derivatives are determined wholly by the large wave-number components of the turbulence. Suppose that we have a turbulence with Reynolds number large enough for the derivative

† $1{\cdot}3u_*$ as an estimate for $\sqrt{u_2^2}$, the r.m.s. turbulent velocity normal to the ground in an atmospheric boundary layer was suggested to us by Wyngaard.

signal to appear intermittent (e.g. the second derivative signal appeared intermittent at $R_\lambda = 830$), then the flatness factor of this intermittent signal depends in part on the signal durations over which the signal is 'zero'. But the statistics of these durations may be associated with the scales of the energy-containing eddies, not the smallest eddies.

Corrsin and Tennekes explored some consequences of simple models, which included intermittency of the fine-structure, and estimated the consequent dependence of the flatness factor of the first derivative on Reynolds number to be $\sim R_\lambda^{1.5}$ and $\sim R_\lambda$, respectively. This experiment shows a dependence weaker than either of those estimates.

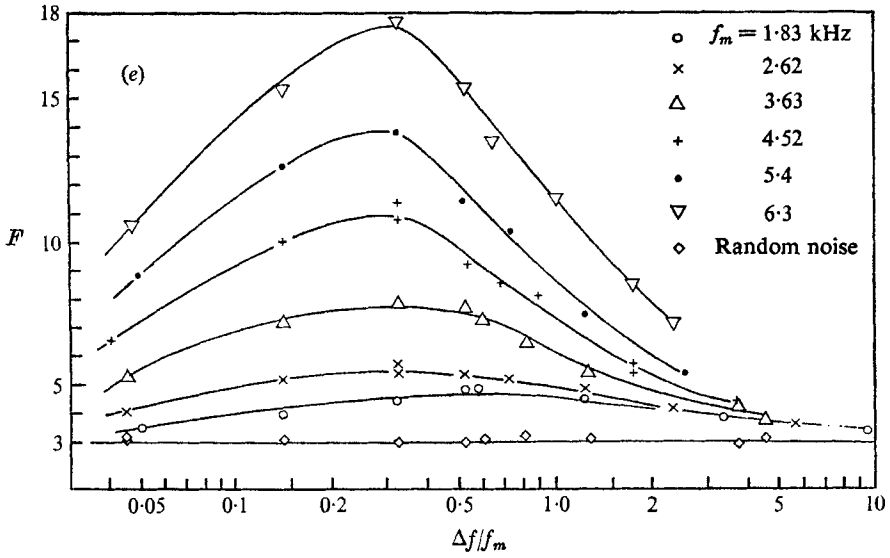

FIGURE 15. Flatness factor of band-pass signal as function of relative bandwidth; grid-generated turbulence with $R_\lambda = 100, f^* = 5{\cdot}9$ kHz.

The Gurvich & Yaglom (1967) model with log-normal distribution of positive random variables predicts that

$$\frac{\langle \phi^K \rangle}{\langle \phi \rangle^K} \sim R_\lambda^{\frac{3}{4}\mu K(K-1)}, \tag{3.3}$$

where ϕ is a non-negative quantity governed by fine-scale components, K is any positive integer, μ is a universal constant empirically estimated to be 0·4 by Gurvich & Yaglom from measured spectra of $(\partial u/\partial t)^2$ and $(\partial w/\partial t)^2$. If we take $\phi = (\partial u/\partial t)^2$ and $K = 2$,we get the flatness factors of the derivatives proportional to $R_\lambda^{0.6}$, which agrees with the high Reynolds number data of the first-derivative signal. The value of μ for the distribution of $(\partial^2 u/\partial t^2)^2$ is not empirically available at present, so no check on the dependence of the flatness factor of $\partial^2 u/\partial t^2$ on R_λ can be made.

The flatness factors of band-pass signals were measured in the grid-generated turbulence at $R_\lambda = 110$ and 86·5. Figure 15 shows the effect of relative band-

width on the flatness factors for a fixed midband frequency. All the curves peak around $\Delta f/f_m = 0{\cdot}3$. F also increases with increasing f_m for fixed $\Delta f/f_m$.

For a given midband frequency, the flatness factor decreases as bandwidth increases from 0·3, because the greater bandwidth passes relatively more low frequency component, which is essentially normal. On the other hand, as Δf decreases toward zero, the filter's time constant must increase; at some Δf the time constant gets larger than the time scale of the on–off cycle of the intermittent signal. Then the filter performs some kind of weighted average on the signal and the flatness factor of the filter output decreases.† With a very narrow-band filter of bandwidth 6 Hz between -3 db points (Hewlett Packard model 302A wave analyzer), it was found that the flatness factors of filtered signals were very close to 3·0 for all midband frequencies.

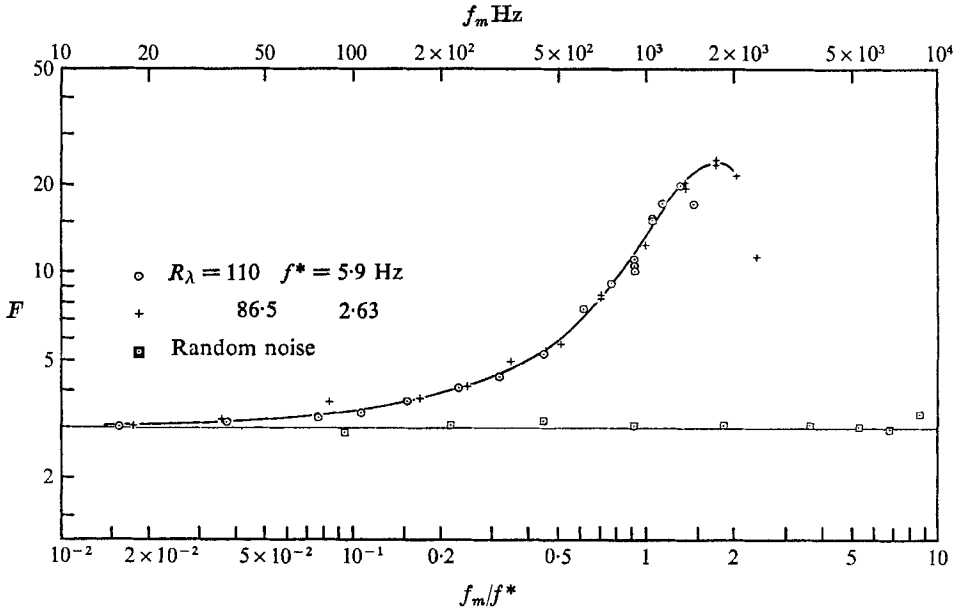

FIGURE 16. Flatness factor of band-pass signal as function of midband frequency, for fixed relative bandwidth $\Delta f/f_m = 0{\cdot}52$; grid-generated turbulence.

To investigate the flatness factors of spectrally local constituents of the turbulent velocity, it is desirable to have a filter as narrow as possible, but not so narrow that the time constant will play a smoothing role. Since F at first increases monotonically with decreasing $\Delta f/f_m$, it seems likely that the levelling off and eventual decrease are a consequence of narrow-band smoothing. Therefore, we chose a working band width $\Delta f/f_m = 0{\cdot}52$, slightly wider than that which gives $F_{\max}$. 0·52 also happens to be the minimum bandwidth of the Krohn–Hite filter.

† It is generally found that any kind of 'smoothing' of a non-normal stationary random variable makes it tend toward normality. In the limit of 'infinite smoothing' this is analogous to the 'Central Limit Theorem' (see Rice 1944, 1945). A more formal version of the 'Central Limit Theorem' for continuous random functions has been presented by Lumley (1970).

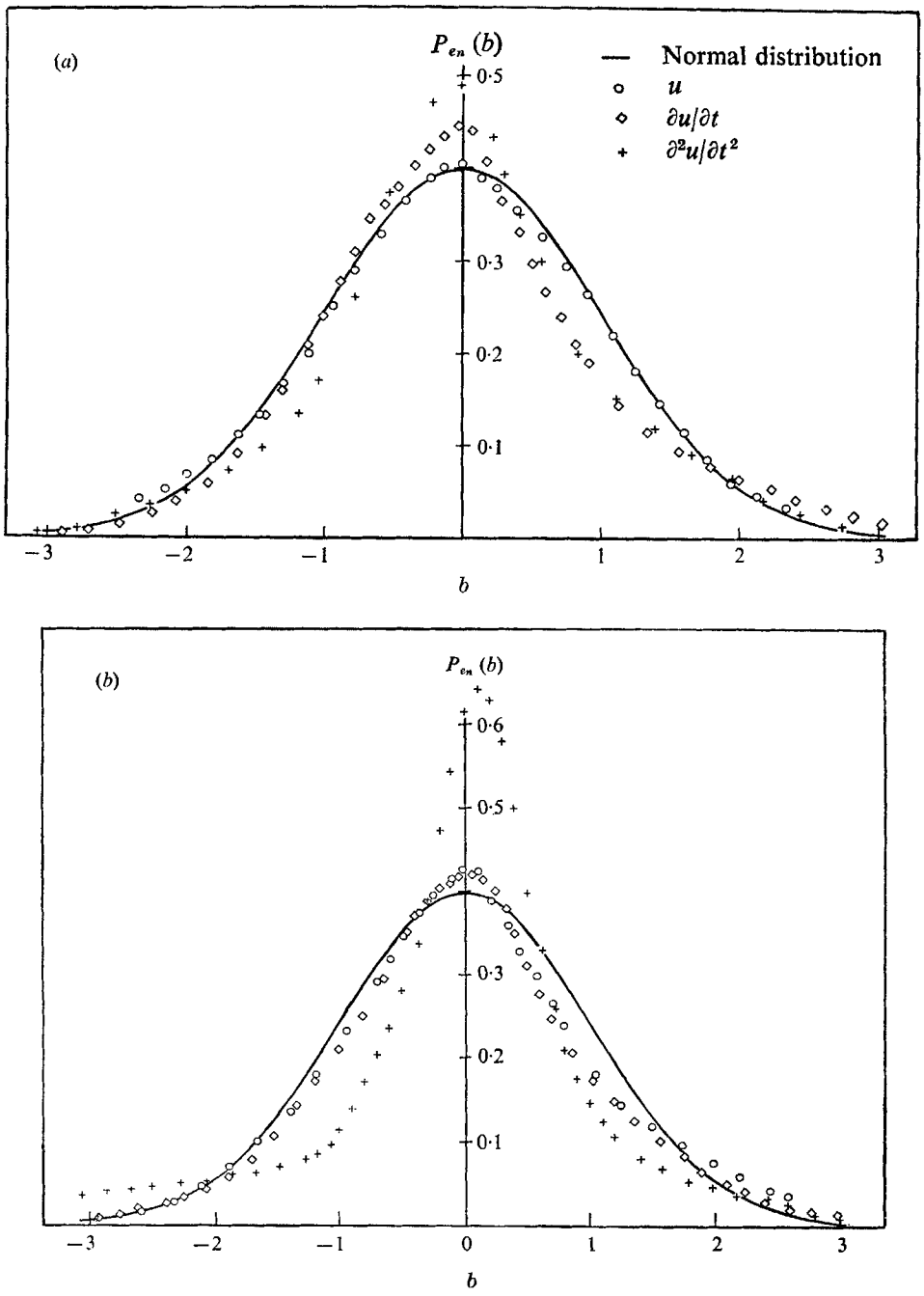

FIGURE 17. Probability densities of u, $\partial u/\partial t$, $\partial^2 u/\partial t^2$ (*a*) in grid-generated turbulence, $R_\lambda = 72$, (*b*) on the axis of a round jet, $R_\lambda = 830$. $e_n^2 = e^2/\langle e^2 \rangle$.

The flatness factors of fixed relative bandwidth signals are shown in figure 16 as functions of midband frequency, f_m/f^*. For the turbulent velocity, the flatness factors start with 3·0 at low f_m and increase monotonically with f_m. For intermittent signals this behaviour would be consistent with the Batchelor–Townsend inference quoted in § 1. The fall-off at very high f_m is associated with the high noise-to-signal ratio at high frequency. The flatness factors of band-passed signals of normal (Gaussian) random noise, shown in figures 15 and 16, are approximately 3·0, independent of both bandwidth and midband frequency.

3.3. *Probability density and distribution function*

If $P_e(a)$ is the probability density function of a random variable $e(t)$, then by definition

$$\int_{-\infty}^{\infty} P_e(a)\,da = 1. \tag{3.4}$$

A conventional way to non-dimensionalize the probability density is with the standard deviation, $\langle e^2\rangle^{\frac{1}{2}}$:

$$\int_{-\infty}^{\infty} \langle e^2\rangle^{\frac{1}{2}} P_e(a)\,d\left(\frac{a}{\langle e^2\rangle^{\frac{1}{2}}}\right) \equiv \int_{-\infty}^{\infty} P_{e_n}(b)\,db = 1. \tag{3.5}$$

Thus, the suitable non-dimensional variables are

$$\left.\begin{aligned} P_{e_n} &\equiv \langle e^2\rangle^{\frac{1}{2}} P_e, \\ \text{and} \qquad e_n(t) &\equiv e(t)/\langle e^2\rangle^{\frac{1}{2}}, \end{aligned}\right\} \tag{3.6}$$

which has a standard deviation of 1·0.

In figures 17(*a*, *b*), the probability densities of u, $\partial u/\partial t$, and $\partial^2 u/\partial t^2$ in a grid-generated turbulence ($R_\lambda = 72$) and on the axis of a round jet ($R_\lambda = 830$), were plotted in these non-dimensional variables. The normal density,

$$P_{e_n}(b) = \frac{1}{\sqrt{2\pi}} \exp\left(-\frac{b^2}{2}\right), \tag{3.7}$$

is included for comparison. Evidently, $u(t)$ is virtually normal, and its derivatives depart from normality. The departure increases with increasing order and with increasing Reynolds number. All deviations from normality are of the same type, tending to have higher probability than the normal curve in the neighbourhood of zero e and at very large values of $e/\langle e^2\rangle^{\frac{1}{2}}$, and to have lower probability at the intermediate values. This is a feature that an intermittent signal should have. If it were exactly zero during the 'off' periods, there would of course be a Dirac function at $e = 0$. The $\partial u/\partial t$ behaviour is consistent with the old data of Batchelor & Townsend (1947) and give a skewness factor $\overline{(\partial u/\partial t)^3}/\overline{(\partial u/\partial t)^2}^{\frac{3}{2}} = -0{\cdot}37$ and $-0{\cdot}076$.

Since the large values of $|e|$ occur only rarely, it is inevitable that the data be least accurate on the 'tails' of the probability density functions. This also makes very risky the business of calculating the higher moments, which weight the

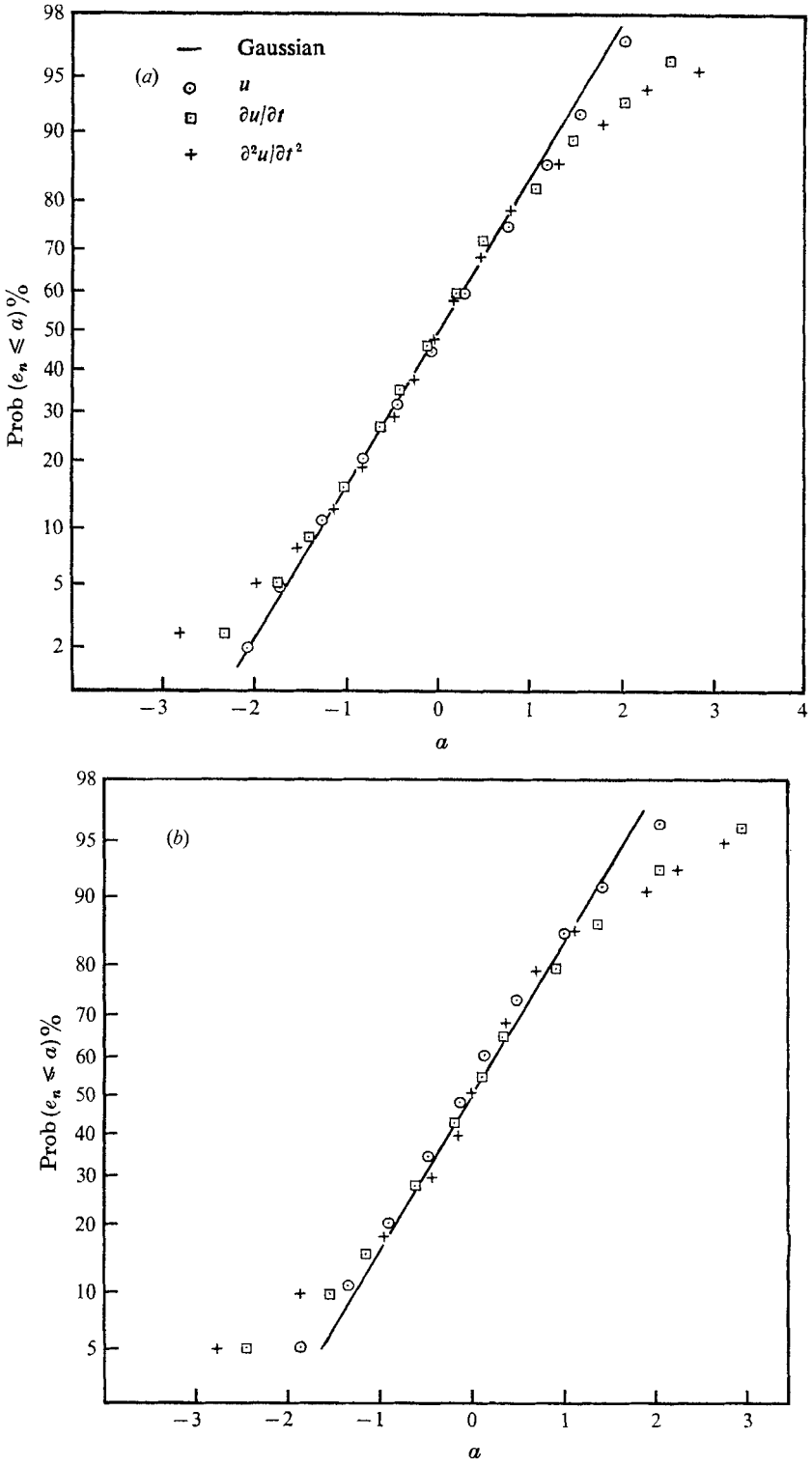

FIGURE 18. Probability distributions of u, $\partial u/\partial t$, $\partial u^2/\partial t^2$ (*a*) in grid-generated turbulence, $R_\lambda = 72$, (*b*) on the axis of a round jet, $R_\lambda = 830$. $f_e = f^*$.

tails heavily, so no estimates on the higher moments based on the probability density data are presented.

Since the directly measured data are the probability distributions, rather than densities, it is easier and more accurate to compare these with the normal distribution function. The probability distribution functions,

$$\text{Prob}\,(e_n \leqslant a) \equiv \int_{-\infty}^{a} P_{e_n}(b)\,db, \tag{3.8}$$

were plotted in a normal probability scale, i.e. a scale on which the normal distribution function would be a straight line.

The probability distributions of u, $\partial u/\partial t$ and $\partial^2 u/\partial t^2$ at $R_\lambda = 72$ and 830 are shown in figures 18(*a*, *b*). We see again that the u's are nearly normal, the derivatives less so.

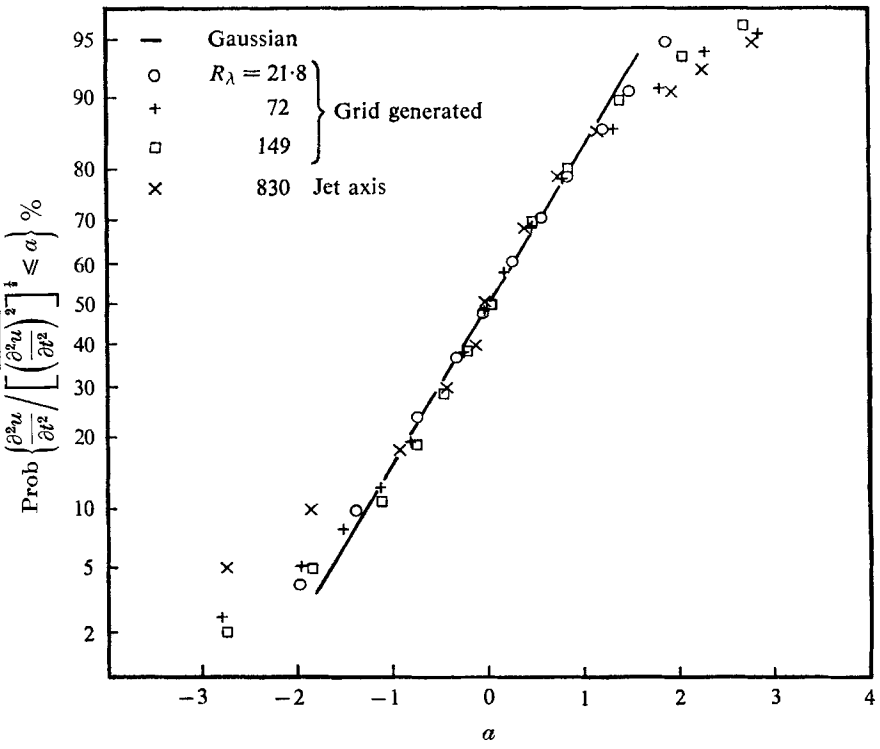

FIGURE 19. Probability distributions of $\partial^2 u/\partial t^2$ at various Reynolds numbers R_λ.

To demonstrate the variation with Reynolds number, probability distributions of $\partial^2 u/\partial t^2$ at various Reynolds numbers are shown in figure 19. $\partial^2 u/\partial t^2$ deviates increasingly from normality as Reynolds number increases.

Next, the probability distribution of various frequency constituents (via band-pass filter) were measured in grid-generated turbulence at $R_\lambda = 110$. They are compared with normal distribution in figure 20, which shows that the low frequency part of the signal has a normal distribution, while the higher frequency parts do not. The deviation from normality increases as frequency increases.

The probability distribution of the signal from the high-pass Butterworth filter,† figure 21, does not agree with normal distribution at all. It departs in much the same way as the band-pass signal with $f_m = 6{\cdot}3$ kHz.

To test Kolmogorov's (1962) conjecture, and Gurvich & Yaglom's (1967) prediction that a non-negative quantity governed by the fine-structure of the motion has a log-normal distribution at large Reynolds numbers, the probability distribution of $e^2(t)$ was computed from that of e, where e is velocity fluctuation, velocity derivative, band-pass or high-pass signal.

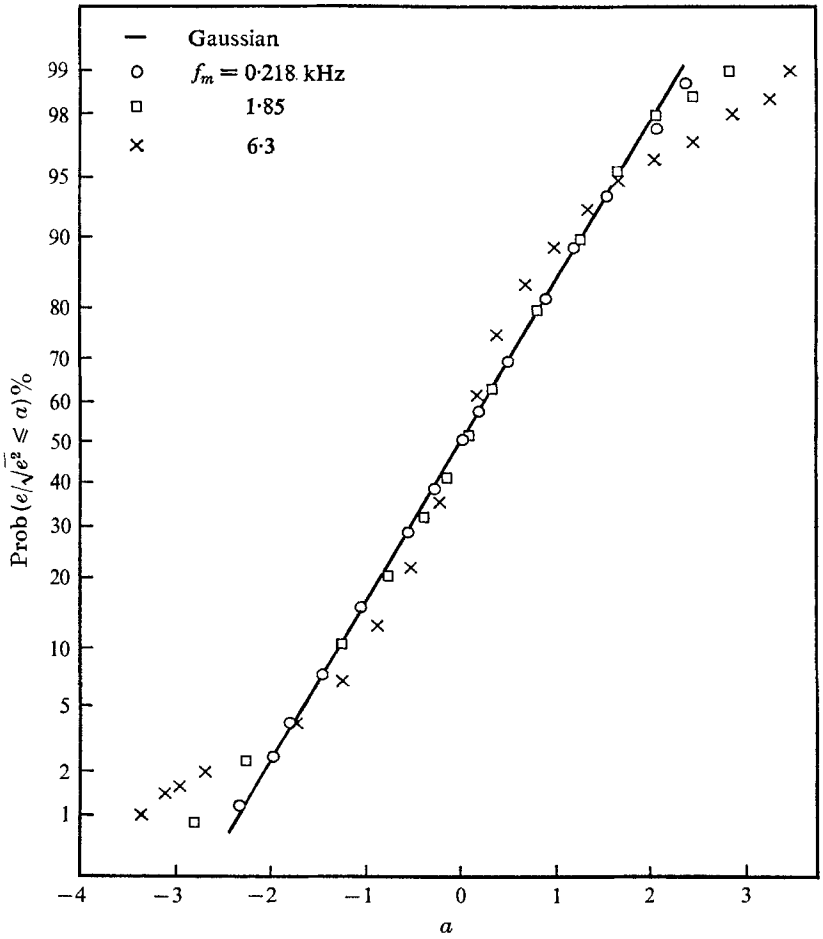

FIGURE 20. Probability distribution of band-pass signals from grid-generated turbulence. $R_\lambda = 110$. Velocity filtered with relative bandwith $\Delta f/f_m = 0{\cdot}52$. f_m is midband frequency.

To compute $P_{e_n^2}$, the probability density function of $e_n^2(t)$, from P_{e_n}, that of $e_n(t)$, we recall the connexion between probability density functions of any two related random variables $r(t)$ and $s(t)$:

$$P_s(b)\,db = P_r\,[a(b)]\,da, \tag{3.9}$$

† Actually, the cascade of the Butterworth filter with all the amplifiers constitutes a band-pass filter. But the high cut-off frequency is so high that the energy spectrum is negligibly small there. Therefore, the band-pass filter is essentially a high-pass filter.

where a represents the values possibly taken on by $r(t)$, and b the values possibly taken on by $s(t)$. $a(b)$ is a mathematical form identical to $r(s)$. In the special case $r \equiv e_n$, $s \equiv e_n^2$ (3.9) gives

$$P_{e_n^2}(b) = \frac{1}{2\sqrt{b}}[P_{e_n}(\sqrt{b}) + P_{e_n}(-\sqrt{b})]. \tag{3.10}$$

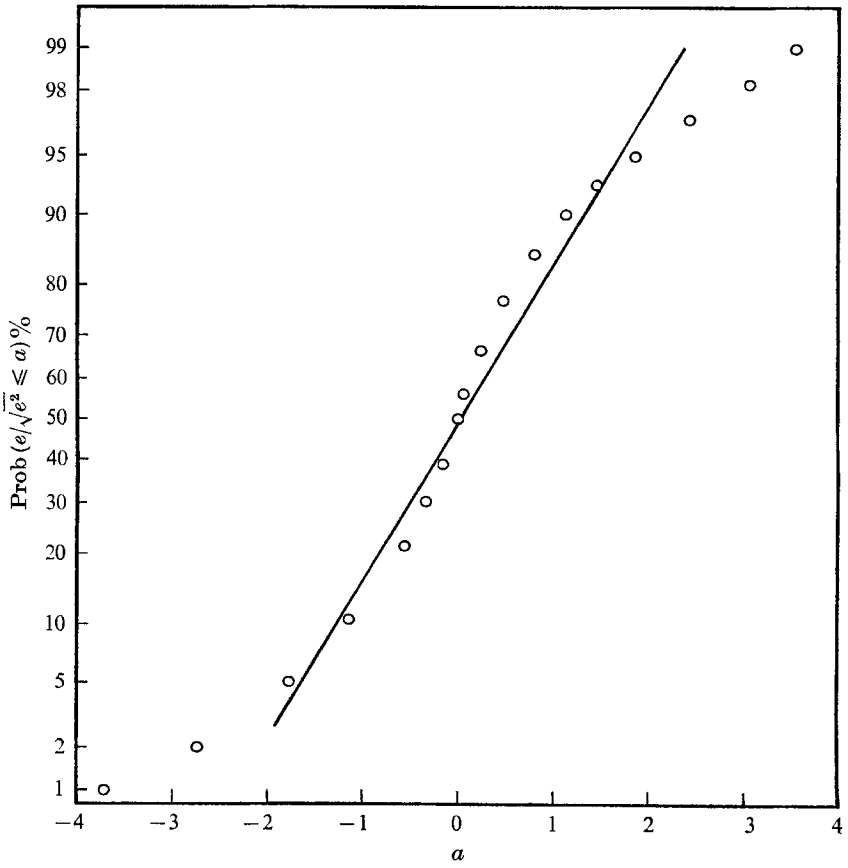

FIGURE 21. Probability distribution of velocity signal through a high-pass Butterworth filter. Low cut-off at 5 kHz. $f_c = f^* = 5{\cdot}9$ kHz. Grid-generated turbulence, $R_\lambda = 110$.

Similarly, we find the distribution function,

$$\text{Prob}\{e_n^2 \leqslant b\} = \text{Prob}\{e_n \leqslant \sqrt{b}\} - \text{Prob}\{e_n \leqslant -\sqrt{b}\}. \tag{3.11}$$

Prob $\{e_n^2 \leqslant b\}$ is plotted on a normal probability scale against $\ln b$, so that 'log-normal distribution functions' would appear as straight lines.

The probability distributions of u^2, $(\partial u/\partial t)^2$ and $(\partial^2 u/\partial t^2)^2$ at $R_\lambda = 72$ and 830 are shown in figures 22(a, b). The results suggest that derivatives of increasing order agree better with log-normality. $(\partial^2 u/\partial t^2)^2$ agrees well over the distribution range 0·35 to 0·9.

To look for a variation with Reynolds number, the probability distributions of $(\partial^2 u/\partial t^2)^2$ at four Reynolds numbers are shown in figure 23. Evidently, the

distribution of $(\partial^2 u/\partial t^2)^2$ is approximated better by a log-normal distribution as Reynolds number increases, although the differences are not really significant for the three larger values.

The probability distributions of the squares of band-pass signals, figure 24(*a*), show that with higher midband frequency, the agreement with a log-normal

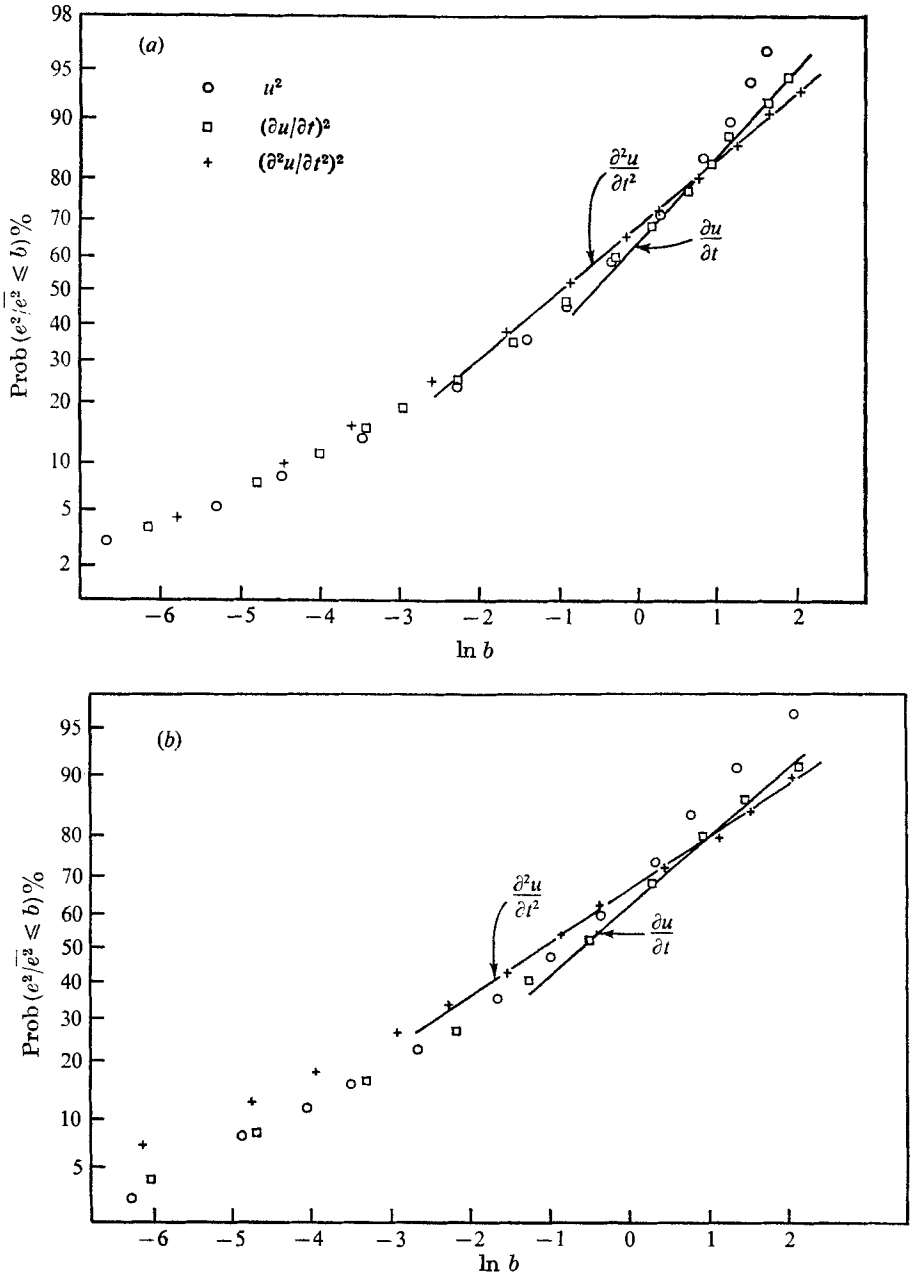

FIGURE 22. Probability distribution of u^2, $(\partial u/\partial t)^2$, $(\partial^2 u/\partial t^2)^2$ compared to log-normal. $f_c = f^*$. (*a*) Grid-generated turbulence, $R_\lambda = 72$. (*b*) Jet axis, $R_\lambda = 830$.

distribution improves. When the amplitude $e/\langle e^2\rangle^{\frac{1}{2}}$ is smaller than $1/\sqrt{33}$, i.e. for distribution function less than 0·3 the distribution departs from log-normality. It should be pointed out that, in the low amplitude range, electronic noise may contribute appreciably, so the turbulence signal may be log-normal over a broader range of values than indicated by these measurements.

The probability distribution of the square of the high-pass signal from a Butterworth filter is shown in figure 24(*b*). This, too, agrees with a log-normal distribution, except in the low amplitude range.

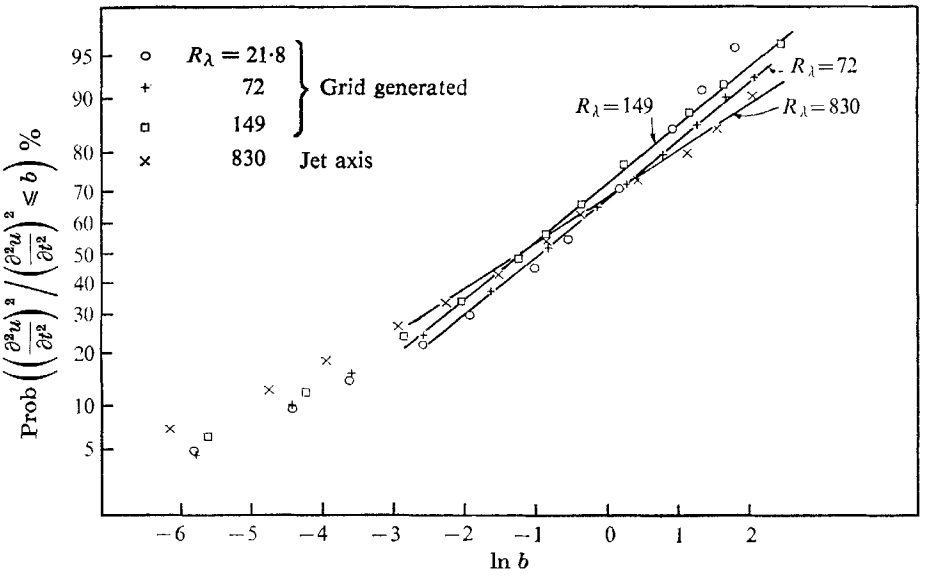

FIGURE 23. Probability distribution of $(\partial^2 u/\partial t^2)^2$, at various Reynolds numbers, compared to log-normal lines.

3.4. *Intermittency characteristics*

It was pointed out earlier that flatness factor departures from the normal value (3·0) do not necessarily indicate intermittency. It is therefore important to measure intermittency factor explicitly. This was done for band-pass signals in grid-generated turbulence and on the axes of round jets. The dependence on Reynolds number was investigated. The bandwidth of the Krohn–Hite filter was set at $\Delta f/f_m = 0{\cdot}52$ and the midband frequency at $f_m = f^*$. Two quantities were measured: the intermittency factor γ, equal to the fraction of space occupied by the fine-structure, and the average number of the fine-structure regions detected by the hot-wire per unit time n. The average width $\langle W\rangle$ of the intercepting chord lines crossing fine-structure regions is

$$\langle W\rangle = \gamma \overline{U}/n, \tag{3.12}$$

where $\overline{U}$ is the mean velocity. The intermittency factor γ and the ratio of $\langle W\rangle$ to the Kolmogorov microscale η are shown in figure 25 as functions of R_λ. Both γ and $\langle W\rangle/\eta$ decrease monotonically with R_λ and seem to reach asymptotic

values at R_λ of the order of several hundreds. This result implies that there is a decrease in the relative fluid volume occuped by fine-structure of given size as the Reynolds number is increased.

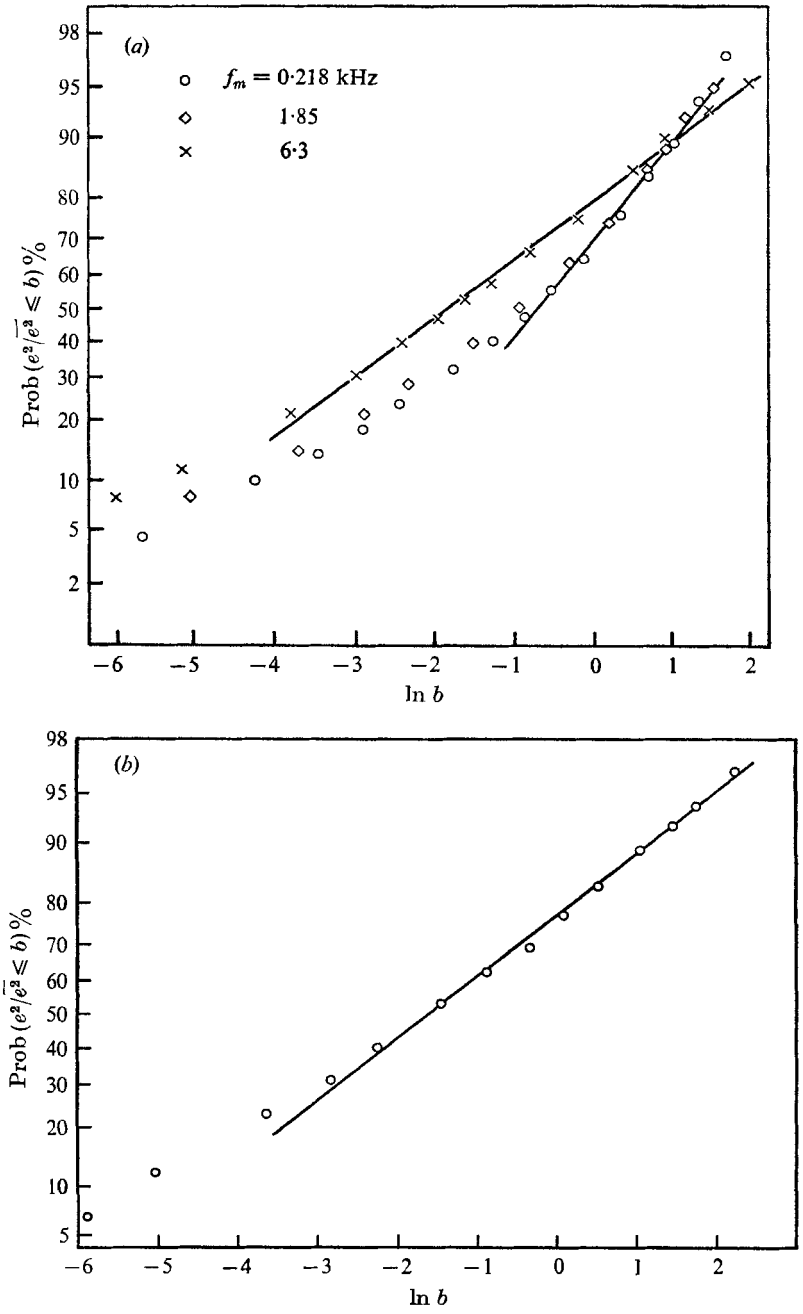

FIGURE 24. Probability distributions of e^2, the square of filtered velocity signals in grid-generated turbulence at $R_\lambda = 110$. $f_c = f^*$. Lines are log-normal. (*a*) Band-pass with $\Delta f/f_m = 0{\cdot}52$; f_m is midband frequency. (*b*) 5 kHz high-pass Butterworth filter.

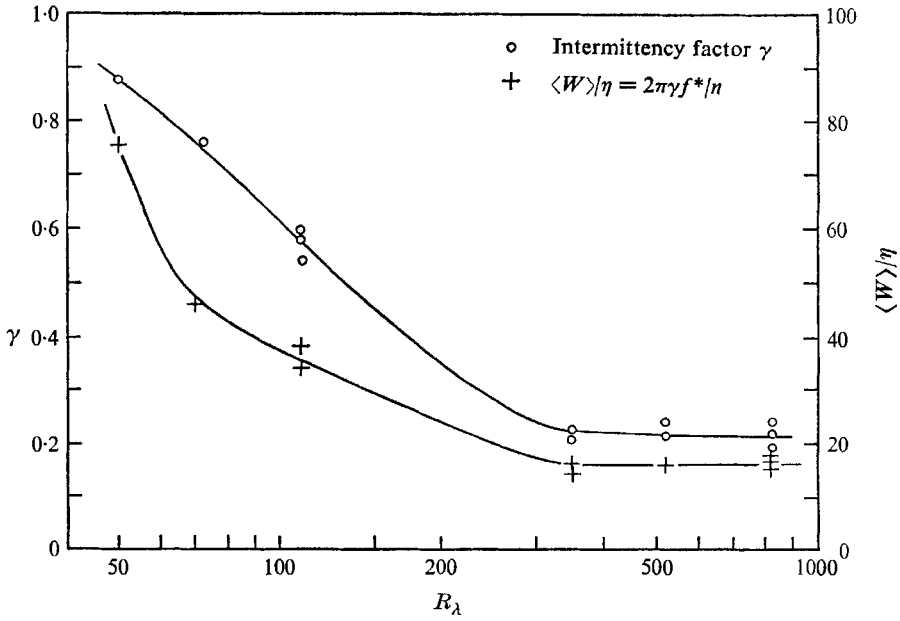

FIGURE 25. Intermittency characteristics of band-pass signals as functions of Reynolds number R_λ, $\Delta f/f_m = 0{\cdot}52$.

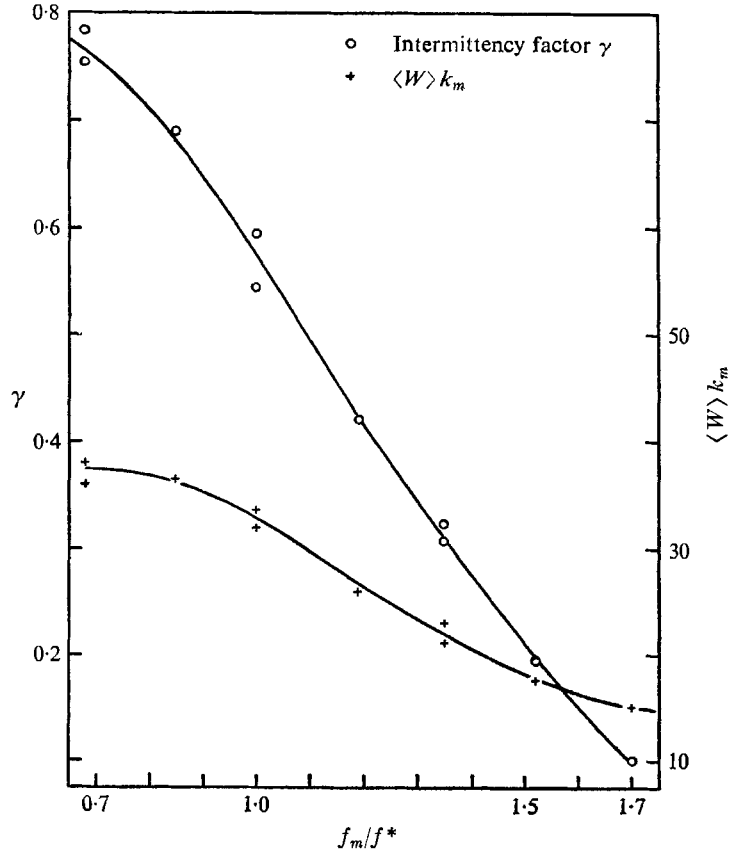

FIGURE 26. Intermittency characteristics of band-pass signals as functions of midband frequency f_m, in grid-generated turbulence, $R_\lambda = 110$. $k_m = 2\pi f_m/U$, $f^* = 5{\cdot}9$ kHz.

In the grid-generated turbulence at $R_\lambda = 110$, the intermittency characteristics of band-pass signals were measured to investigate possible dependence on wave-number, assuming the Taylor approximation. The filter bandwidth was $\Delta f/f_m = 0{\cdot}52$. The intermittency factor γ and the non-dimensional width $\langle W \rangle k_m$, where $k_m = 2\pi f_m/\overline{U}$, are shown in figure 26 as a function of f_m/f^*. $\langle W \rangle k_m$ is a measure of the ratio of an average linear dimension of fine-structure containing regions to the size of the particular 'narrow-band' fine-structure used to identify them (i.e. with which they are 'active'). For $R_\lambda = 110$, both γ and $\langle W \rangle k_m$ decrease monotonically with increasing f_m/f^*, hence with increasing k_m. The former means that the relative fluid volume occupied by eddies with size of order k_m^{-1} decreases with increasing k_m, which is consistent with a suggestion of Batchelor & Townsend (see § 1). The latter means that, for fixed R_λ, the linear dimension of a fine-structure region $\langle W \rangle$ decreases relative to the 'eddy size' k_m^{-1}, which identifies (or activates) it, for smaller and smaller eddy sizes (fine-structure).

From the numerical values of $\langle W \rangle k_m$ in figure 26, we see that, over the full range of fine-structure examined ($0{\cdot}7f^* \leqslant f_m \leqslant 1{\cdot}7f^*$), the domains of fine-structure are much larger than the fine-structure itself: $15 \leqslant \langle W \rangle k_m \leqslant 35$.

Batchelor & Townsend (1949) suggested $\gamma F = 3{\cdot}0$ (equation (3.2)) for the relationship between the flatness factor and intermittency factor of an intermittent variable. γ and F of the band-pass signal ($\Delta f/f_m = 0{\cdot}52$, $f_m = f^*$) in a grid-generated turbulence ($R_\lambda = 110$) were measured to be 0·58 and 13, respectively. $\gamma F = 7{\cdot}5$ differs significantly from 3·0. Of course, $\gamma F = 3{\cdot}0$ assumes intermittent signals whose high-intensity state is normal, and whose low-intensity state is zero. The departure here may be associated with violation of either assumption, or both.

We thank W. George for his help in the laboratory, J. P. Cavelle and M. Cuneo for their help in numerical computations, and O. Guillon for assembling some of the electronic circuits. This work was supported by the U.S. National Science Foundation under Grant GK 10268, and by the Office of Naval Research under Contract 4010(05). Their support is much appreciated. The paper is adapted from part of Kuo (1970).

Appendix. Some properties of the log-normal probability distribution function

In order to take into account the large spatial non-uniformities of turbulent energy dissipation rate, Oboukhov (1962) and Kolmogorov (1962) proposed a modified version of the original universal similarity hypothesis. The modification involved the assumption that the logarithm of the energy dissipation rate has a normal distribution. Gurvich & Yaglom (1967) devised a theory for this, in the sense that they offered more primitive hypotheses which yielded the prediction that any non-negative quantity (e.g. energy dissipation rate) governed by fine-scale components has a log-normal probability distribution function.

The possible log-normality has been tested experimentally by several investigators (Gurvich & Yaglom 1967; Sheih 1969; Stewart, Wilson & Burling 1970; Gibson, Stegen & Williams 1970; Wyngaard & Tennekes 1970), but no unique way of curve fitting has been used up to now. Furthermore, no detailed discussion of the behaviour of a log-normal density function has been given. In this appendix, the method used in § 3.3 to try to fit the data with log-normal curves is described, and some moments of the log-normal density are compared with direct measurements. The behaviour of a log-normal density function is discussed, including its implication for intermittency.

A 'log-normal probability distribution' is one for which the logarithm of the (non-negative) random variable ϵ has a normal probability distribution, i.e.

$$P_{\ln\epsilon}(y) = \frac{1}{\sqrt{2\pi\beta}}\exp\left[-\frac{(y-m)^2}{2\beta^2}\right], \tag{A 1}$$

where $m = \langle \ln\epsilon \rangle$, and $\beta^2 = \langle (\ln\epsilon - m)^2 \rangle$.

We can compute arbitrary moments. Write $y = \ln\epsilon$; then $dy/d\epsilon = 1/\epsilon$ and, letting c be the possible value of ϵ,

$$P_\epsilon(c) = P_{\ln\epsilon}[y(c)]\, dy/dc;$$

thus,
$$P_\epsilon(c) = \frac{1}{\sqrt{2\pi\beta c}}\exp\left[-\frac{(\ln c - m)^2}{2\beta^2}\right]. \tag{A 2}$$

The Kth moment of ϵ is

$$\langle \epsilon^K \rangle = \int_0^\infty \frac{1}{\sqrt{2\pi\beta c}}\, c^K \exp\left[-\frac{(\ln c - m)^2}{2\beta^2}\right] dc;$$

thus,
$$\langle \epsilon^K \rangle = \exp(mK + \tfrac{1}{2}K^2\beta^2). \tag{A 3}$$

In particular,
$$\langle \epsilon \rangle = \exp(m + \tfrac{1}{2}\beta^2) = \exp\langle \ln\epsilon \rangle \exp(\tfrac{1}{2}\beta^2).$$

It is convenient to non-dimensionalize. Write $\epsilon_n = \epsilon/\langle\epsilon\rangle$. Then the p.d.f. of this normalized variable is

$$P_{\epsilon_n}(z) = \langle\epsilon\rangle P_\epsilon(\epsilon_n\langle\epsilon\rangle);$$

thus,
$$P_{\epsilon_n}(z) = \frac{1}{\sqrt{2\pi\beta z}}\exp\left[-\frac{(\ln z + \beta^2/2)^2}{2\beta^2}\right]. \tag{A 4}$$

The distribution function is

$$\text{Prob}\{\epsilon_n \leqslant s\} = \int_0^s \frac{1}{\sqrt{2\pi\beta z}}\exp\left[-\frac{(\ln z + \beta^2/2)^2}{2\beta^2}\right] dz;$$

thus,
$$\text{Prob}\{\epsilon_n \leqslant s\} = \int_{-\infty}^{\ln s} \frac{1}{\sqrt{2\pi\beta}}\exp\left[-\frac{(y + \beta^2/2)^2}{2\beta^2}\right] dy, \tag{A 5}$$

where
$$y = \ln z.$$

Equation (A 5) on normal probability paper, with $\ln s$ as amplitude variable, gives a family of straight lines because it is a normal distribution for $y \equiv \ln\epsilon_n$, with parameter β. The mean is $-\frac{1}{2}\beta^2$ and the variance is β.

A way to see how closely a set of probability distribution data points may be approximated by a log-normal distribution is to try to fit these data points with

a straight line on a normal probability paper with amplitude plotted in a logarithmic scale. There are two parameters to be adjusted in choosing the 'best' straight lines: (i) β, which determines the slope,

$$2\beta = (\ln S_{0\cdot84}) - (\ln S_{0\cdot16}),$$

where $S_{0\cdot16}$ and $S_{0\cdot84}$ are the values such that

$$\text{Prob}\{\epsilon_n \leqslant S_{0\cdot16}\} = 0\cdot16,$$

(the probability that a normal variable is less than the negative of its variance)

$$\text{Prob}\{\epsilon_n \leqslant S_{0\cdot84}\} = 0\cdot84,$$

(the probability that a normal variable is less than its variance), (ii) $\langle\epsilon\rangle$, which determines the location of the straight line. Different choices of $\langle\epsilon\rangle$ only add a constant to $\ln\epsilon_n$, shifting the straight line parallel to itself.

In the actual curve fitting for § 3.3, β was chosen so that the straight line would fit as many data points as possible. The mean $\langle e^2\rangle$ of the non-negative random variable was used as $\langle\epsilon\rangle$ to non-dimensionalize the variable e^2 for convenience; no attempt was made to determine the best $\langle\epsilon\rangle$, since different choices of $\langle\epsilon\rangle$ only translate the straight line horizontally. If the data were truly log-normally distributed, then $\langle e^2\rangle = \langle\epsilon\rangle$, so $\langle e^2\rangle$ would be the best choice for $\langle\epsilon\rangle$; the straight line would be one of the family with $\ln\epsilon_n$ having a mean of $-\frac{1}{2}\beta^2$ and a variance of β.

In figure 24(*b*), for example, the straight line corresponds to a log-normal distribution with $\beta = 2\cdot1$. Then, according to (A 5),

$$\ln e_m^2/\langle\epsilon\rangle = \ln S_{0\cdot5} = -\beta^2/2 = -2\cdot2,$$

where e_m^2 is the median of e^2. But this high-pass signal e^2 is non-dimensionalized by $\langle e^2\rangle$ in figure 24(*b*), and the straight line has

$$\ln e_m^2/\langle e^2\rangle = \ln S_{0\cdot5} = -0\cdot16;$$

thus,
$$\ln\langle\epsilon\rangle/\langle e^2\rangle = 0\cdot6 \quad \text{or} \quad \langle\epsilon\rangle = 1\cdot82\langle e^2\rangle. \tag{A 6}$$

Similarly, the probability distribution of the band-pass signal with $\Delta f/f_m = 0\cdot52$ and $f_m = 6\cdot3\,\text{kHz}$ in figure 24(*a*) shows

$$\langle\epsilon\rangle = 1\cdot68\langle e^2\rangle. \tag{A 7}$$

Both of these ratios $\langle\epsilon\rangle/\langle e^2\rangle$ depart appreciably from 1·0, the value required for a log-normal distribution. As a further check, we note that, if e^2 were log-normal, then the flatness factor of e would be

$$F \equiv \frac{\langle e^4\rangle}{\langle e^2\rangle^2} = \frac{\langle\epsilon^2\rangle}{\langle\epsilon\rangle^2} = \frac{\exp(2m+2\beta^2)}{\exp(2m+\beta^2)} = \exp(\beta^2). \tag{A 8}$$

The band-pass signal data in figure 24(*a*) give F equal to about 80–100 ($f_m = 6\cdot3\,\text{kHz}$). Direct measurement, on the other hand, gives 16.

The fact that a log-normal distribution predicts much larger second and (especially) fourth moments than are observed suggests that the large values of the actual e^2 are far less probable than would be required by log-normality. This deviation at large amplitude was also reported by Stewart, Wilson & Burling (1970).

To see how a log-normally distributed random variable might appear inter-

mittent, we examine some features of the probability density function (A 4). The peak is located by setting

$$dP_{\epsilon_n}(z)/dz = 0. \tag{A 9}$$

With (A 4), this gives

$$(\epsilon_n)_{\max} = \exp(-\tfrac{3}{2}\beta^2), \tag{A 10}$$

and

$$P_{\epsilon_n}[(\epsilon_n)_{\max}] = \frac{1}{\sqrt{2\pi\beta}} \exp(\beta^2), \tag{A 11}$$

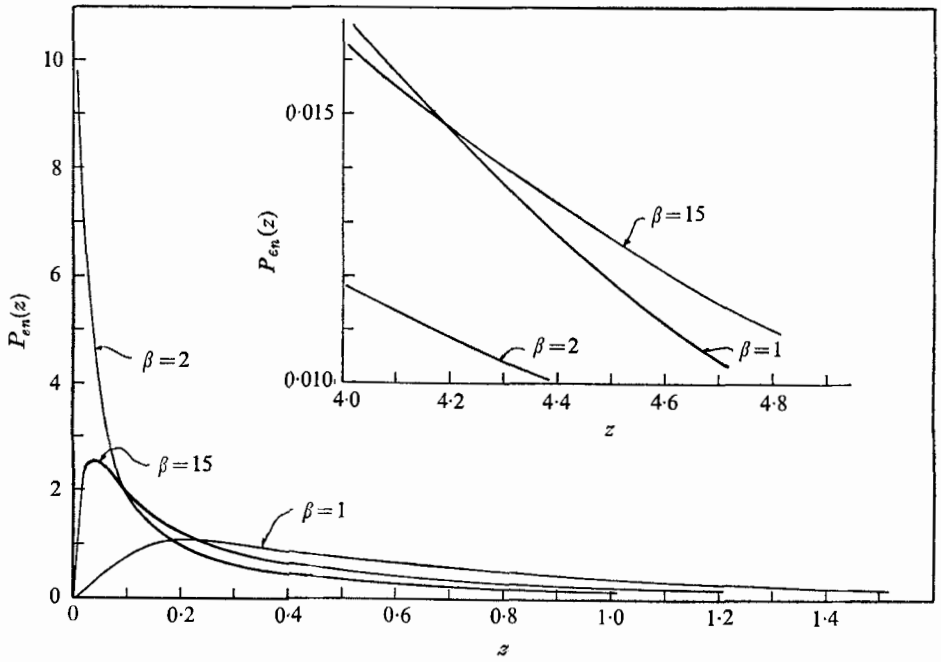

FIGURE 27. Log-normal probability density curves.

where $(\epsilon_n)_{\max}$ is the location at which $P_{\epsilon_n}(z)$ is maximum. Equations (A 10) and (A 11) show that the peak of the probability density function will increase rapidly, and its ϵ-location will move toward zero as β increases. This extreme peak near $\epsilon_n = 0$ is certainly consistent with a signal which spends a lot of its time near zero. Of course, if this time is not in relatively extended periods, the signal will still not appear to be intermittent.

Another ramification is shown by the sign of $\partial P_{\epsilon_n}/\partial\beta$. From (A 4),

$$\frac{\partial P_{\epsilon_n}}{\partial\beta} = \frac{1}{(2\pi)^{\frac{1}{2}} z} \exp\left[-\frac{(\ln z + \beta^2/2)^2}{2\beta^2}\right]\left[-\frac{1}{\beta^2} - \tfrac{1}{4} + \frac{(\ln z)^2}{\beta^4}\right];$$

thus,

$$\frac{\partial P_{\epsilon_n}}{\partial\beta} > 0, \quad \text{if} \quad (\ln z)^2 > \frac{\beta^4}{4} + \beta^2,$$

i.e. if $\epsilon_n > \exp((\beta^4/4+\beta^2)^{\frac{1}{2}})$, or $\epsilon_n < \exp(-(\beta^4/4+\beta^2)^{\frac{1}{2}})$,

and $\partial P_{\epsilon_n}/\partial\beta < 0$, if $\exp(-(\beta^4/4+\beta^2)^{\frac{1}{2}}) < \epsilon_n < \exp((\beta^4/4+\beta^2)^{\frac{1}{2}})$.

Therefore, as β increases, the probability density at very large and very small values of ϵ_n will increase and that at intermediate values of ϵ_n will decrease. Some log-normal probability density curves with various β are shown in figure 27, and they suggest that the random variable will appear intermittent if β is large enough.

REFERENCES

BATCHELOR, G. K. & TOWNSEND, A. A. 1947 *Proc. Roy. Soc.* A **190**, 534.

BATCHELOR, G. K. & TOWNSEND, A. A. 1949 *Proc. Roy. Soc.* A **199**, 238.

BATCHELOR, G. K. 1953 *The Theory of Homogeneous Turbulence.* Cambridge University Press.

BRADSHAW, P. 1967 *Nat. Phys. Lab. Aero. Rep.* 1220.

CHAMPAGNE, F. H., HARRIS, V. G. & CORRSIN, S. 1970 *J. Fluid Mech.* **41**, 81.

COMTE-BELLOT, G. 1965 *Ecoulement Turbulent Entre Deux Parois Paralleles.* Paris: Publ. Sci. et Tech. du Min. de l'Air.

COMTE-BELLOT, G. & CORRSIN, S. 1966 *J. Fluid Mech.* **25**, 567.

COMTE-BELLOT, G. & CORRSIN, S. 1971 *J. Fluid Mech.* **48**, 273,

CORRSIN, S. 1958 *NACA Res. Memo* 58B11.

CORRSIN, S. 1962 *Phys. Fluids*, **5**, 1301.

FISHER, M. J. & DAVIES, P. O. A. L. 1964 *J. Fluid Mech.* **18**, 97.

GIBSON, C. H., STEGEN, G. R. & MCCONNELL, S. 1970 *Phys. Fluids*, **13**, 2448.

GIBSON, C. H., STEGEN, G. R. & WILLIAMS, R. B. 1970 *J. Fluid Mech.* **41**, 153.

GIBSON, M. M. 1963 *J. Fluid Mech.* **15**, 161.

GURVICH, A. S. & YAGLOM, A. M. 1967 *Phys. Fluids*, **10** (suppl.), 59.

GURVICH, A. S. & ZUBKOVSKII, S. L. 1963 *Izs. Acad. Sci. USSR. Geophys. Ser.* **12**, 1856.

HESKESTAD, G. 1965*a* *J. Appl. Mech.* **32**, 721.

HESKESTAD, G. 1965*b* *J. Appl. Mech.* **32**, 735.

KENNEDY, D. A. & CORRSIN, S. 1961 *J. Fluid Mech.* **10**, 366.

KOHAN, S. M. 1969 Ph.D. thesis, Stanford University.

KOLMOGOROV, A. N. 1941 *C.R. Acad. Sci.* (*Doklady*), *USSR*, **30**, 301.

KOLMOGOROV, A. N. 1962 *J. Fluid Mech.* **13**, 81.

KOVASZNAY, L. S. G. 1947 *NACA Tech. Mem.* 1130.

KUO, A. Y.-S. 1970 Ph.D. Thesis, Johns Hopkins University.

LANDAU, L. D. & LIFSHITZ, E. 1959 *Fluid Mechanics.* (Trans J. B. Sykes & W. H. Reid.) Addison-Wesley. (1944, 1st Russian edn., Moscow.)

LIEPMANN, H. W. 1952 *J. Appl. Math. Phys.* **3**, 321.

LUMLEY, J. L. 1965 *Phys. Fluids*, **8**, 1056.

LUMLEY, J. L. 1970 *Stochastic Tools in Turbulence.* Academic.

NOVIKOV, E. A. 1963 *Prikl. Math. Mech.* **27**, 944.

NOVIKOV, E. A. & STEWART, R. W. 1964 *Izv. Acad. Sci. USSR. Geophys. Ser.* **3**, 408.

OBOUKHOV, A. M. 1962 *J. Fluid Mech.* **13**, 77.

POND, S. & STEWART, R. W. 1965 *Izv. Acad. Sci. USSR, Atmos. and Oceanic Ser.* **1**, 914

RICE, S. O. 1944 *Bell Syst. Tech. J.* **23**, 282.

RICE, S. O. 1945 *Bell Syst. Tech. J.* **24**, 46.

ROSE, W. G. 1962 *J. Appl. Mech.* **29**, 554.

SAFFMAN, P. G. 1970 *Phys. Fluids*, **13**, 2193.

SANDBORN, V. A. 1959 *J. Fluid Mech.* **6**, 211.

SHEIH, C. M. 1969 Ph.D. thesis, Pennsylvania State University.

SHEIH, C. M., TENNEKES, H. & LUMLEY, J. L. 1971 *Phys. Fluids*, **14**, 201.

STEWART, R. W., WILSON, J. R. & BURLING, R. W. 1970 *J. Fluid Mech.* **41**, 141.

TENNEKES, H. 1968 *Phys. Fluids*, **11**, 669.

TOWNSEND, A. A. 1948 *Aust. J. Sci. Res.* A, **1**, 161.

WYNGAARD, J. C. 1967 Ph.D. thesis, Pennsylvania State University.

WYNGAARD, J. C. & TENNEKES, H. 1970 *Phys. Fluids*, **13**, 1962.

WYGNANSKI, I. & FIEDLER, H. E. 1970 *J. Fluid Mech.* **41**, 327.

YAGLOM, A. M. 1966 *Soviet Phys.* **11**, 26.

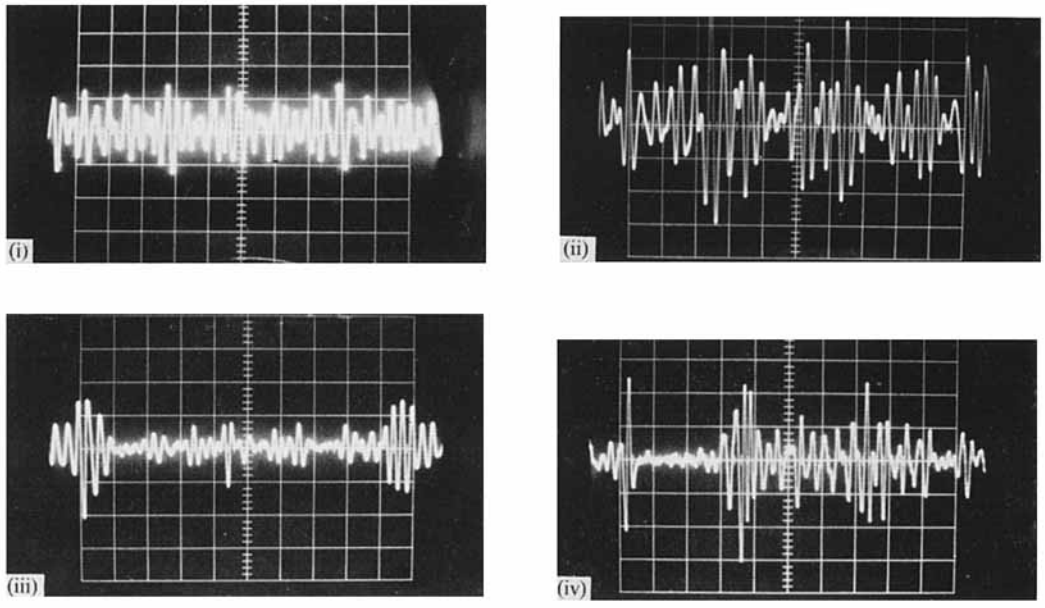

(*a*)

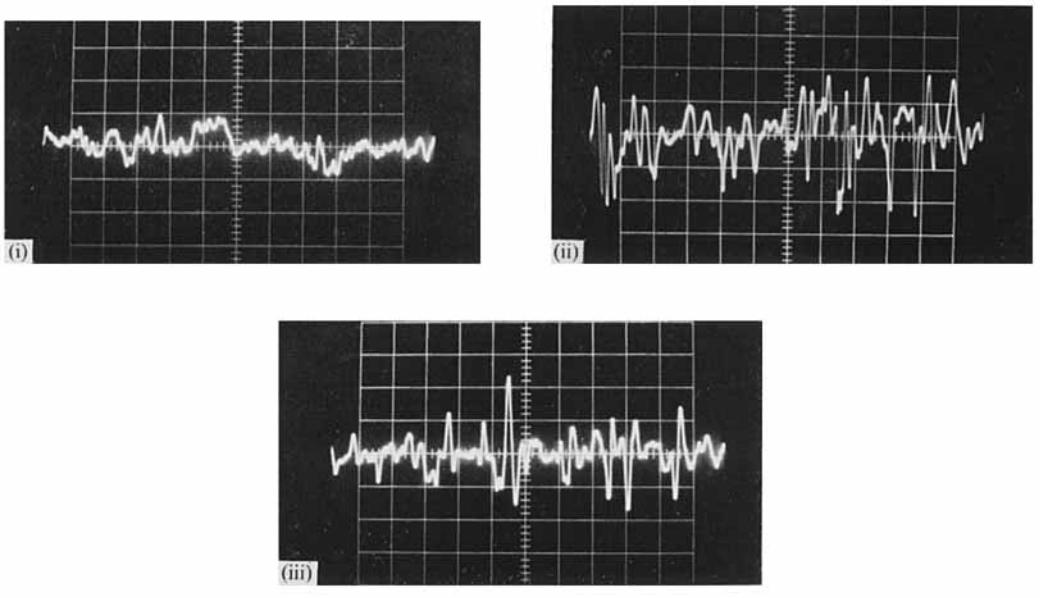

(*b*)

FIGURE 11. Oscillograms. Grid-generated turbulence ($R_\lambda = 110, f^* = 5{\cdot}9\,\text{kHz}$). (*a*) Of band- and high-pass signals from a wire: (i) $f_m = 200\,\text{Hz}$, $\Delta f/f_m = 0{\cdot}52$, 20 ms/division (horizontal scale); (ii) 1 kHz, 0·52, 4; (iii) 6, 0·52, 1; (iv) high-pass signal, $f_c = 5\,\text{kHz}$, 1 ms/division. (*b*) Of velocity fluctuation and time derivatives: (i) $u(t)$, 4 ms/division; (ii) $\partial u/\partial t$, 2; (iii) $\partial^2 u/\partial t^2$, 1.